2013

Photoluminescence, Dual-Donor Energy Transfer And Single X-Ray Crystallographic Studies Of Eu3+ Andtb3+ Complexes With Pyridines And Triazaphosphaadamantane Oxide (Tpao) Ligands

Derick Akaju Forcha

North Carolina Agricultural and Technical State University

Photoluminescence, Dual-donor Energy Transfer and Single X-ray Crystallographic Studies of Eu^{3+} andTb^{3+} complexes with pyridines and triazaphosphaadamantane oxide (TPAO) ligands

Derick Akaju Forcha

North Carolina A&T State University

A thesis submitted to the graduate faculty

in partial fulfillment of the requirements for the degree of

MASTER OF SCIENCE

Department: Chemistry

Major: Chemistry

Major Professor: Dr. Zerihun Assefa

Greensboro, North Carolina

2013

School of Graduate Studies
North Carolina Agricultural and Technical State University
This is to certify that the Master's Thesis of

Derick Akaju Forcha

has met the thesis requirements of
North Carolina Agricultural and Technical State University

Greensboro, North Carolina
2013

Approved by:

_____	_____
Dr. Zerihun Assefa Major Professor	Dr. Alex Williamson Committee Member
_____	_____
Dr. Margaret Kanipes-Spinks Department Chairperson	Dr. William Adeniyi Committee Member

_____

Dr. Sanjiv Sarin
Dean, The Graduate School

Biographical Sketch

Derick Akaju Forcha was born on April 18, 1979, in Buea, Cameroon, Graduated Bilingual Grammar School in 1999, and received the Bachelor of science degree from North Carolina Agricultural & Technical State University in 2010. He is a candidate for the Masters of Science degree in Chemistry.

Dedication

This thesis is dedicated to my father, John Nkemazem Forcha

Acknowledgements

That I may attain University Education, let alone realizing a project of this magnitude, I thank God Almighty for the strength and wisdom to undertake this research. I sincerely wish to express my endless gratitude to my Advisor Dr. Zerihun Assefa, for his support. I also want to give thanks to my parents; my mom, Angelina B. Forcha and my dad, Mr. John N. Forcha, who introduce and took me through qualitative education during the formative years of my life.

I was also assisted and encouraged by persons to whom it is but germane to extend endless thanks, Dr. William Adeniyi, Dr. Alex Williamson, Dr. Darkus Jenkins, Dr. Matthew Mickens, Kendra Whitehead, Carlos Crawford, Sharen Selvy, Cyril Forcha, Julius Ngwa. I am also very indebted to Dr. Margaret Kanipes, for her support. I thank all the faculty members of the Department of Chemistry.

Table of Contents

List of Figures

List of Tables

List of Symbols

Å	Angstrom
EtOH	Ethanol
MeOH	Methanol
mL	Milliliter
PH_3	Phosphine
UV	Ultraviolet
Ln	Lanthanides
nm	Nanometer
IR	Infrared Spectroscopy
ptpy	4', 4''''- (1-4 phenylene) bis (2, 2':6', 2-terpyridine)
ppz	Pyridino [2-3-b] pyrazine
bbterp	6,6″-Dibromo-2,2′:6′,2″-terpyridine
tppz	2,3,5,6-tetra(2'-pyridyl)pyrazines
TPA	1,3,5,-triaza-7-phosphatricyclo[3.3.1.1] decane
TPAO	1, 3, 5,-triaza-7-phosphatricyclo [3.3.1.1] decane-7-oxide

Abstract

Coordination of several chromophoric ligands capable of sensitizing Tb^{3+} and Eu^{3+} ions have been studied. Four new complexes of Eu^{3+} and Tb^{3+} ions were achieved by coordinating Eu with 4', 4''''- (1-4 phenylene) bis (2, 2':6', 2-terpyridine) , pyridino [2-3-b] pyrazines and 6,6″-dibromo-2,2′:6′,2″-terpyridine.The crystal structure of $[Tb(TPAO)_2(H_2O)_4(Au(CN)_2)_3]$, was determined and shows a polymeric three-dimensional coordination with a monoclinic space group Cc, Z=4. The unit cell parameters are a = 17.4266(14) Å, b = 10.8224(10) Å, c = 18.0270(16) Å, $\alpha = 90°$ $\beta = 109.309(3)°$ $\gamma = 90°$. The structure exhibits an equilateral Au-Au-Au interaction bridged to a terbium core by the C-N groups. Three other complexes, viz $[Eu(ppz)_2(H_2O)_n]Cl_3$, $[Eu(ptpy)(H_2O)_n]Cl_3$ and $[Eu(bbterp)(H_2O)_n]Cl_3$, have also been synthesized and characterized using IR and luminescence spectroscopy, although no crystal was obtained suitable for X-ray diffraction analysis. The ligand tetra(2'-pyridyl)pyrazine (tppz) was also crystallized and its crystal structure solved. The results herein, elaborate the mode of dual donor sensitization from ligand groups to the lanthanide ions. The efficiency of energy transfer that occurs in the Ln^{3+} complexes has been calculated, taking into account the radiative and non radiative relaxation processes, and the limitation encountered. A broad excitation spectrum at 369, 366 and 380 nm were observed for $[Eu(ppz)_2(H_2O)_n]Cl_3$, $[Eu(bbterp)(H_2O)_n]Cl_3$ and $[Eu(ptpy)(H_2O)_n]Cl_3$ complexes, respectively upon monitoring the Eu^{3+} emission indicating the presence of ET in a donor-acceptor type interaction.

CHAPTER 1

Introduction

1.1 Coordination Chemistry

The formation of metal complexes, ultimately requires the interaction (and bond formation) of metal centers and either neutral or negatively charged molecules called ligands. More succinctly, these complexes are formed when ligands or Lewis basis are bonded to acceptor molecules – Lewis acids by means of electron lone pairs, and these ligand atoms that are directly bonded to metal centers are referred to as the donor atoms [1]. Such complex formation requires a wide array of parameters, for the reaction to be plausible, some of these aspects include, the chemical environment in which the reaction will occur, the molar ratio of the metal as well as the ligands, the coordination number of the metal center, the solubility of reactants, thereby existing as ions in solution, the structure of the ligands and steric hindrance, as well as the size of the cation and the chemistry of the solvent are relevant factors that need to be taken into account when designing a plausible synthesis for the formation of complexes.

Efforts in our research group have been on the systematic characterization of complexes of rare earths ion and a mechanistic understanding of their behavior in both solid and liquid state, and of the internal charge transfer that coexist between the metal and the ligands with the aim of understanding the sensitization and efficiency of the sensitization processes that exist in this type of complexes.

1.2 Lanthanides Overview

A group of 14 elements at bottom row of the periodic table often referred sometimes to as the ‘rare earth ‘ or lanthanoids, range from Cerium to lutetium, do have a similar gradation in both physical and chemical properties,(with some exceptions) across the period and thus their

electronic configuration goes from Ce ($4f^1\ 5d^1\ 6s^2$) to Lu ($4f^{14}\ 5d\ 6s^2$) , further, these Ln^{3+} are all relatively electropositive, thus behaving as hard acids [2]. Most lanthanides, in their room temperature modification, crystallize in either the cubic or hexagonal close packed arrangement; exceptions being Sm (rhombohedral) and Eu (body centered cubic) [2]. Lanthanide contraction, remains a significant non-periodic physical property thus implying a decrease in Ln^{3+} ionic radius with increase atomic number [2, 3].

1.2.1 The Lanthanides Contraction (Atomic Radii). Across the lanthanides series from lanthanum to lutetium, the atomic radii decreases [2]. The 4 f-electrons are "inner" electrons in that, the maximum of their charge density functions is well inside the outermost ($5s^2 5p^6$) electrons; thus they are shielded from the surroundings of the lanthanide ion accounting for the limited dependence of f-f spectra of complexes of ligand [2, 3]. The 5s and 5p orbitals, however, penetrate the 4f subshell and thus are not shielded from the increasing nuclear change, contracting as the lanthanide series is traversed [4, 5].

1.2.2 Characteristics of Lanthanides. A similarity in physical properties throughout the series with the adoption of predominantly the +3 oxidation state and the prevalence of high coordination numbers usually 8-9, further, the coordination is largely determined by steric rather than crystal-field considerations; non-directional bonding, and thus shows the tendency to a decrease in coordination number across the series as the radius of the lanthanide ion decreases [2, 3, 6]. A preference for 'hard' donor atoms (such as O, F), binding in order of electronegativity and exhibit very small crystal-field effects [4, 6]. And Sharp 'line-like' electronic spectra of complexes which show little dependence on ligands and the magnetic properties of a given ion again largely independent of environment, and thus ionic complexes are more likely to undergo rapid ligand-exchange [4, 5].

1.3 Lanthanide Complexes

A unique feature of lanthanide complexes is the large contribution of electrostatic effects to the metal ligand bonding, since the 4f valence orbitals of the trivalent lanthanide ions are well shielded from the environment by the filled 5s and 5p orbitals, the 4f orbitals do not participate in the bonding and as such the metal-ligand bond is largely ionic, and covalent contributions can be safely neglected in this regard [7].

1.3.1 Luminescence of Ln^{3+} Ions. Trivalent lanthanide ions display fascinating optical properties. Many high-technology applications of lanthanide-containing materials such as energy-saving lighting devices, displays, optical fibers and amplifiers, lasers, responsive luminescent stains for biomedical analyses and cell sensing and imaging, heavily rely on the brilliant and pure-color emission of lanthanide ions [8, 9].

1.3.2 Absorption. Lanthanide ions in the +3 oxidation state do have absorption spectra that have low molar extinction coefficients and consist of very narrow lines, which can be attributed to intra-4*f* transitions [6]. Their low intensity is implicit on the fact that these transitions are forbidden by selection rules. Infact the 4*f* electrons are embedded in the element's core, and are thus shielded by the 5*s* and 5*p* orbitals [10].

1.3.3 Emission. Lanthanide ions do have light emission capabilities, this is based on *f*-*f* transitions and it has two relevant properties as a consequence. The narrow emission bands of lanthanide ions can emit characteristic bright colors. The emission transitions are electric-dipole forbidden and therefore the most efficient way to obtain lanthanide emission is by using sensitizers [8, 11].

1.3.4 Europium. The element europium, atomic number 63 is a lanthanide, with an electronic configuration of [Xe] $4f^7 6s^2$ and exist predominantly in the +3 oxidation state. Its

compounds present several important properties and applications. Due to narrow f–f transitions, a good sensitization of the Eu^{3+} luminescence can be achieved through the antenna effect [12, 13]. The lines of the emission spectra are generally sharp and dependent on the crystal field around the metal ions. This fact may be used in the determination of the symmetry and geometry of complex species, and in some cases in species containing other elements, when they are doped with europium acting as a structural probe and thus increasing attention has been paid to the luminescence of europium compounds [14].

1.3.5 Terbium. The element Terbium, with atomic number 65, occurs at the bottom row of the periodic table and has electronic configuration [Xe] $4f^9 6s^2$ is a ductile silvery white and malleable air stable element, and enjoys the usual +3 and +4 oxidation states, the Tb^{3+} cation, is very luminescent, under UV light, though the +3 oxidation state is most prominent, luminescence of Tb^{3+} complexes is characterized by emission from the $^5D_4$ state resulting in green luminescence [2, 6, 15]. Terbium compounds have found widespread use in special lasers and as phosphors that produce the green color in television tubes and computer monitors, and also in the fabrication of high-definition X-ray screens [16]. Terbium and europium do have characteristic line-like spectra, which could be assigned to various transitions originating from the excited state to the ground state of their respective tri positive ions, for instance, for Tb^{3+} ions, the transitions arise from the $^5D_4$ excited state to the various low lying ^7F_J states, meanwhile the luminescent transitions of europium thus arise from the $^5D_0$ excited state to the various low lying ^7F_J states, further tri positive terbium can form complexes with various organic chromophores and can thus show energy transfer from the lanthanide to the ligand or vice versa, the illustration of the various transitions for both the Eu^{3+} and Tb^{3+} ions can be seen in figure 1.1 and 1.2 respectively [15, 17].

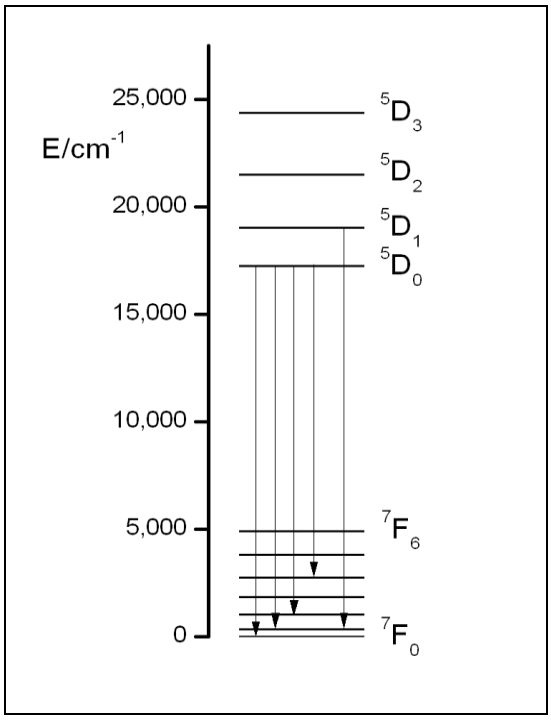

Figure 1.1. The line spectrum of Eu^{3+} ion

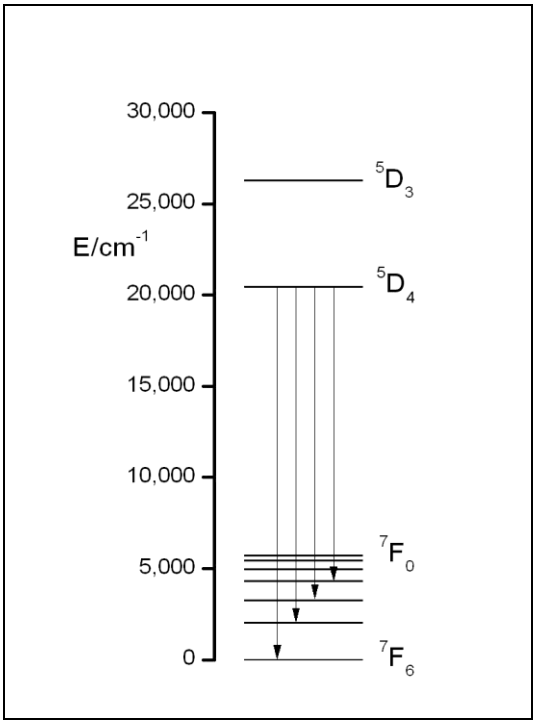

Figure 1.2. The line spectrum of Tb^{3+} ion

1.4 Sensitization

The usual impediment in lanthanide-ion systems is that direct absorption of the f−f excited states is very inefficient, hence, a light-harvesting ligand is essential to enhance the emission from the metal cation site [12].

To overcome the problem of weak f-f oscillator strengths when exciting the luminescent lanthanide ions, energy is often transferred from the surroundings of the metal ion (either an inorganic matrix or an organic ligand, in a stepwise mechanism: light absorption from the surroundings, transfer onto the lanthanide ion, and the resulting emission of light. The overall process is complex and involves several mechanisms and energy levels.

Its optimization is important to the overall luminescence yield that can be attained, and in addition to providing an efficient path for the excitation of lanthanide ions, this sensitization process has also the advantage that now the "Stokes' shifts" are very large, which allows an easy spectral separation of the remaining matrix luminescence from the metal ion emission. Modeling of this complex process is now at hand for coordination compounds [8].

In solution, organic chromophores remain attached to the metal center as a sensitizer [15]. The emission from the excited state Ln^{3+} ions is characterized by narrow emission bands in the NIR to UV range and long emission lifetimes, up to milliseconds, characteristic of the individual metal ion [15]. Døssing further affirms that these characteristics are caused by the parity forbidden, and in many cases spin forbidden, nature of the 4f _ 4f transitions and the fact that the 4f electrons, being effectively shielded by 5p and 6s electrons, are not involved in chemical bonding [8, 15]. This is an important consideration of ln^{3+} coordination in solution.

Some ligands such as the terpyridine molecules have proven to act as donors that absorb in the UV region of the electromagnetic spectrum, and have shown to undergo energy-

transfer processes with select lanthanide cations and therefore, act as light-harvesting antennae and can subsequently transfer absorbed energy to coordinated Ln^{3+}cations [5, 12, 18].

1.4.1 Jablonski and efficient sensitized luminescence in Ln^{3+} ions. The first three energy levels, are the ground singlet state , the first excited singlet state and the lowest triplet state, all have relevant roles in determination of the photo physical properties of the (ligands) antenna [19]. The Ln^{3+} ion is represented here by ground and two excited energy levels, with their energy values, close to the energy of the triplet state of the antenna [19]. The ^{1}S and ^{3}T represents the singlet and triplet states respectively of the ligands, which then undergoes some decay process either by fluorescence F or phosphorescence P, or through non-radiative NR pathways [15, 20]. Inter-system crossing (ISC) between the two states and energy transfer ET leads to population of the Ln^{3+} ion excited state f* . Following this process,the excited state of the Ln^{3+} decays by luminescence. BT is back-energy transfer, that can happen if the triplet state of the ligand and the excited state of the lanthanide cation are close in their energy levels [21].

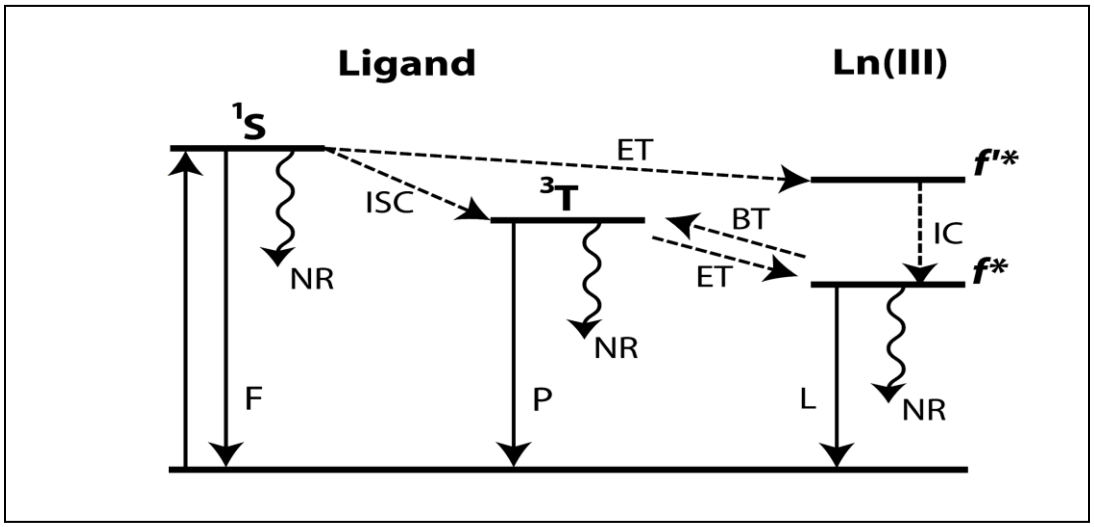

Figure 1.3. The Jablonski diagram showing energy transfer pathways from Ln^{3+} and ligands

1.5 Ligands

Ligands are molecules or ions that have the ability to coordinate to a metal cation to form coordinated compounds, known as complexes. Ligands can have various capabilities; they can act as mondentate, bidentate, bridging, chelating, macro cyclic and or polydentate ligands amongst other attributes, depending on the nature of ligand molecule in question. In this work, our ligands of interests are both inorganic as well as organic polyatomic molecules with nitrogen and oxygen donor atoms, and fall under the broader class of the pyridines. These pyridines have unique physical and chemical attributes, that make them, useful in forming charge transfer complexes, with metal centers such as lanthanides [4, 5, 8, 18]. Polynuclear metal complexes with aromatic nitrogen heterocycles as bridging ligands have been desirable for use in the study of photo-induced applications, extraction reagents and specific catalytic reactions, further, the design of these metal complexes requires N-donor bridging ligands having two or more sets of coordination (polydentate) sites to incorporate molecular components [18]. The following ligands, have been explored extensively for this purpose, 2,3,5,6-tetra(2‘-pyridyl)pyrazine (tppz), terpyridine, TPAO amongst others.

1.5.1 Pyridines and Pyrazines. Pyridine is a conjugated cyclic organic compound, with a chemical formula of C_5H_5N, it is similar to benzene in structure, the exception being that one C-H group is replaced by a nitrogen atom, this molecule however, is planer as shown by electron diffraction studies and show resonance similar to benzene [22]. Ligands used here include: 6,6″-dibromo-2,2′:6′,2″-terpyridine, and 4’, 4’’’’- (1-4 phenylene) bis (2, 2’:6’, 2-terpyridine). Similar to Pyridines, are pyrazines, they however differ in that instead of a C-H bond replacement by Nitrogen in the benzene ring, there is actually two nitrogen replacement on the benzene ring, and has the molecular formula of $C_4H_4N_2$, the presence of Nitrogen in these

compounds makes them very useful in both organic and inorganic synthesis [22]. Considering these compounds have nitrogen atoms with lone electron pairs, makes it plausible for these compounds to act as potential electron donors. Further, derivatives of these rings and a combination thereof, are of interest to this research, as exemplified by 2, 3, 5, 6-tetra (2‘-pyridyl) pyrazines and Pyridino [2-3-b] pyrazines.

1.5.2 Tetra(2‘-pyridyl)pyrazine. The multi-ring heterocycle 2,3,5,6-tetra(2‘-pyridyl)pyrazine (tppz) was first reported by Goodwin and Lions in 1959 [23, 24]. The compound 2,3,5,6-tetra(2‘-pyridyl)pyrazine (tppz) is a remarkably versatile electron donor that displays a wide variety of binding modes. Recent work by Padgett and others, indicates that about 14 low energy conformations of tppz have been identified, noting a preference for some conformations in different solvent [23]. A review of previously reported crystal structures of complexes containing tppz as a ligand, reveals a variety of tppz binding modes, including mono-, bi-, and tridentate coordination to a variety of Lewis acids [23]. This ligand has been shown to adopt both chelating and bis(chelating) coordination modes, and thus has the ability to form mononuclear as well as poly nuclear complexes [23]. A variety of structural motifs, including chain and framework structures are possible, making this ligand an attractive choice in attempts to prepare porous compounds based on the assembly of organic molecules and metal-ion building blocks, such supramolecular systems have received much attention lately, especially due to their potential as functional materials [25].

1.5.3 Phosphine Oxides. Phosphine oxides are organophosphorus compounds with the general formula $R_3P=O$, R could represent either a Hydrogen atom or an alkyl or aryl functionality, they thus are utilized extensively as ligands in organometallic chemistry. phosphine compounds are sought after as ligands for transition metal complexes as well as in

lanthanide complexes because of their strong binding properties and to a lesser extent their steric advantages and as such these ligands are particularly useful in applications where robust transition metal / Lanthanide–phosphine complexes are employed [26] further, these Phosphine ligands are strong σ-donors, and their electronic, steric, and stereo chemical properties vary based on the substituent's attached to the phosphorus atoms and choosing the correct phosphine ligands for a metal complex allows control over the electronic and steric environment of the complex ,this tunability amongst other attributes is what makes the phosphines a very useful ligand for optimization in complex formation and as such a plethora of phosphine-containing ligands have been synthesized for use in lanthanide coordination [26], including TPA and TPAO which have been previously synthesized by our research group. The phosphine oxide, TPAO, is relevant to mitigate the quenching effect of water molecules, due to the O-H vibrational modes and owing to its much smaller cone angle, gives it a unique capability to compete and knock off water molecules that may attach to the lanthanide ion in the complexation process.

1.6 Luminescence

The electromagnetic nature of light, the environment of a luminescent molecule and even the molecular structure of the emitting molecule are relevant aspects that cause certain molecules to absorb or emit light. The absorption process is important to cause subsequent emission, from a luminescent molecule [27]. Thus luminescence is the ability of a substance that occurs from electronically excited states, and could be of two types, namely; fluorescence and phosphorescence [10]. In this regard, electron in the excited singlet states are paired to the second electron in the ground state orbital, coupled with the possibility that return to the ground state is spin allowed and occurs by emission of a photon much more rapidly [10]. To fully understand the concept of fluorescence and to illustrate the various molecular processes that can

occur in excited states , it is relevant to consider a brief overview of the Jablonski diagram [10]. Contrary to internal conversion and intersystem crossing, excited molecules may remain in the lowest vibrational level of the lowest excited singlet state for about 10^{-10} - 10^{-7} s and subsequently emit UV or visible fluorescence [27].

1.6.1 Fluorescence. Excited molecules, upon light absorption are said to arise from same vibrational level from the ground state and terminate in the various vibrational levels of the electronically excited state, thus having the geometry of the equilibrium ground state, this is the Franck-Condon excited state [10, 27]. Amongst the various processes, such as intersystem crossing and internal conversion, the excited molecule may remain in the lowest vibrational level of the lowest excited singlet state for a period of about 10^{-10} - 10^{-7} s and subsequently emit UV or visible fluorescence [27]. Florescent molecules typically show lifetimes of the order of 10^{-8} s, fluorescence actually occur within the time frame, typical of electronic transitions, that is about 10-15 s, thus causing insufficient time for vibrational relaxation to occur during the transition, except in cases where the ground state of the molecule has the same equilibrium geometry as the lowest excited singlet state, in such situations, the fluorescing molecule may arrive in a vibrationally excited level of the ground electronic state even if the emission originated from the lowest vibrational level of the lowest excited singlet state [10, 27].

1.6.2 Phosphorescence. A process that exist in triplet excited states when light is emitted, and in which case the electron in the excited orbital has the same spin orientation as the ground state electron [10]. Phosphorescence, can be looked upon as a delayed response as opposed to Fluorescence, further it is a radiative decay process from the ground state , from a state of different multiplicity, it is also a slow and spin-forbidden process, in a phosphorescent complex, upon initial excitation, the complex usually populates a state by a spin-allowed

transition, and this process, is most likely to occur in molecules with restricted vibrational freedom [6, 27].

Further the resulting red emission of Eu^{3+} is a direct consequence of transitions from its $^5D_0$ state to all of the lower lying ^7F_J levels as exemplified on the figure below [11, 17, 28-30].

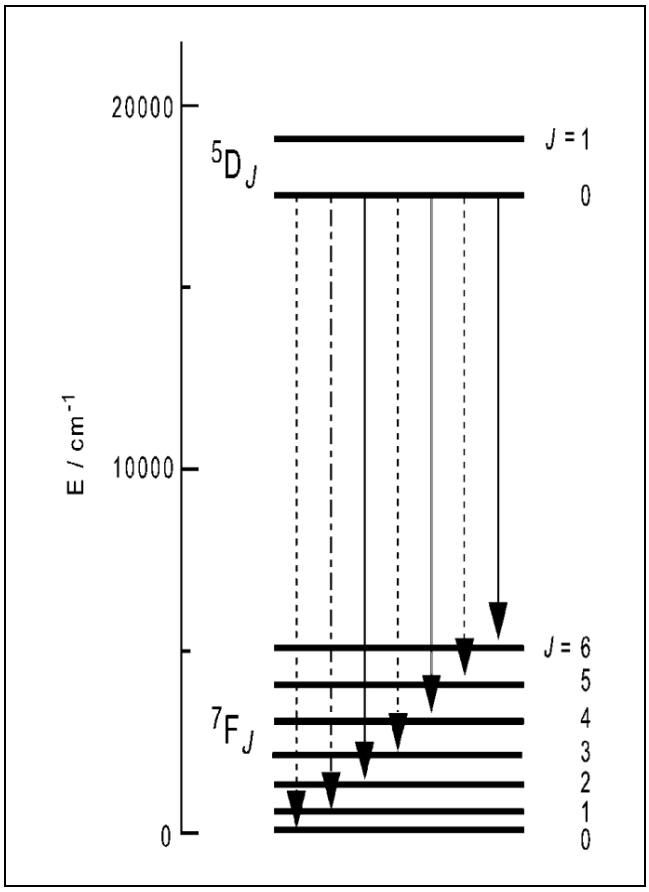

Figure 1.4. Term schemes for the Eu^{3+} transitions between the $^5D_0$ state and the ^7F_J manifold.

CHAPTER 2

Experimental Methods

2.1 Chemical Reagents

The chemicals used in this study include amongst others methanol, ethanol, toluene, diethyl ether, hydrogen peroxide, acetonitrile, DMSO, DMF, TPAO, TPA, $EuCl_3 \bullet 6H_2O$, $TbCl_3 \bullet 6H_2O$, $KAu(CN)_2$ and various pyridine/pyrazine ligands. The following reagents and solvents where purchased from Sigma Aldrich and were used without further purification.

2.2 Designing a Plausible Synthesis (Theory)

Considering the fact that ligands containing oxygen and nitrogen donor atoms are very promising in bonding with lanthanide 3+ ions, it becomes imperative to consider the hydration and coordination number of the lanthanide species, when designing a plausible synthesis, with respect to Europium and Terbium 3+ ions, that has coordination number of 8 and 9, the number of nitrogen and or oxygen donor atoms on the ligands must amount to 8 or 9, in order to avoid the possibility of water molecules, to coordinate on to the lanthanide species, in this case, TPAO,(acting as a subsequent ligand) with a smaller cone angle, can certainly replace, and void water molecule in the complexation process, hence the quenching ability of water molecules is greatly avoided, and quenching can be minimized. Other aspects that are relevant are steric hindrance of the ligand species, metal-ligand molar ratios and the solubility and polarity of solvents, in which case non polar solvents would be theoretically good for this reactions owing to the fact that donor atoms such as nitrogen and oxygen atoms will become more harder bases [2, 3, 5]. Further, the hard acid and soft acid and bases principle is a very important point of contention and should not be neglected when designing a plausible synthesis for the formation of lanthanide complexes.

2.2.1 Synthesis of tppz. Interestingly, attempts to coordinate tppz, resulted in the formation of the ligand crystal complex in solution, as a result, an experimental procedure was established. In which in a 25 mL beaker, 0.05 g of Europium triflate trichloromethane sulfonate was dissolved in 10 mL THF, and stir for 10 min to achieve complete dissolution. The sample was let stand for slow evaporation after about one week, fine square crystals where harvested, suitable for single X-ray crystallography.

2.2.2 Synthesis of TPAO from TPA. TPAO was synthesized from TPA according to literature method using 0.5 g, (3.2×10^{-3}mol) of TPA dissolved in 20 mL of methanol. A 0.5 mL of hydrogen peroxide solution (30% in ethanol), was added onto the TPA mixture using Pasteur pipette. The resulting solution, which contained a small amount of white precipitate, was stirred for about 20 min. And was kept in the fume hood for slow evaporation and the resulting product was recrystallized using hot ethanol [31].

2.2.3 Synthesis of $[Tb(TPAO)_2(H_2O)_4(Au(CN)_2)_3]$. In a 50 mL Pyrex round bottom flask, 8.0 mL of chloroform was siphon into the round bottom flask, using a syringe, 0.0360 g (equivalent to I molar) of $TbCl_3 \bullet 6H_2O$, was added into the solvent and 0.031g of KAu $(CN)_2$ (equivalent to 1 molar) and 0.0281 g of TPAO (equivalent to 1.70 molar) was added, then 5.0mL of MeOH was added, and finally 4.0 ml of CH_3CN was also added. The reaction mixture was stirred while refluxing via a steady flow of cold water for 6 hours. After refluxing 2.0 mL of diethyl ether was added and let stand – using slow evaporation technique. After about one month tiny crystals where harvested suitable for single X-ray diffraction.

2.2.4 Synthesis of $[Eu(ptpy)(H_2O)_n]Cl_3$. In a 20 mL beaker, 0.026 g of $EuCl_3 \bullet 6H_2O$, was dissolved in 3.0 mL Ethanol, while stirring, meanwhile on a separate 20 mL beaker, 0.005 g of ptpy was dissolve in 5.0 mL chloroform, and stirred separately until complete dissolution, and

finally after 10 min, both solutions where combined and stirred further for 15 min. After which the reaction vessel was placed in the fume hood for slow evaporation. After about one week, the solid product that was collected at the bottom of the beaker was analyzed using photoluminescence and IR spectroscopic techniques.

2.2.5 Synthesis of $[Eu(bbterp)(H_2O)_n]Cl_3$. In a 20 mL test tube, 0.0529 g of bbterp, was dissolved in 2.0mL dichloromethane, after which 0.058 g of $EuCl_3.6H_2O$ was added to the test tube, followed by 1.0 mL Ethanol and 1.0 mL DMSO, the resulting solution was then agitated using sonication for 7 min. The final product was let to stand for slow evaporation. After about 3 weeks, fine crystalline material was recovered and dried on a filter paper. The product was characterized using luminescence and IR spectroscopies.

2.2.6 Synthesis of $[Eu(ppz)_2(H_2O)_n]Cl_3$. To a 10.0 mL test tube, a 0.053 g of $EuCl_3.6H_2O$, 0.045 g of TPAO, and 0.0193 g of ppz where all added and 2.0 mL of distilled water was used to dissolve all reactants. The solution was shaken well for 5 min, and to let stand for slow evaporation and crystallization. After about six weeks, small brownish crystals, suitable for single x-ray diffraction where observed and was harvested for characterization using single X-ray diffraction.

2.3 Spectroscopic Methods

The characterization of the research samples where done using various techniques, amongst the spectroscopic methods used where UV-VIS spectroscopy and IR spectroscopies. For the IR samples, approximately 0.05 g of the desired product was ground with a mortar and pestle, to form a fine powder. The sample was then carefully placed on the sample holder. The IR instrumentation was a Mattson 2020 Galaxy Series Fourier- Transform Infrared spectrophotometer with a wavelength range capability of (350-4000cm^{-1}). A 300MHz Varian

NMR 300-411149FT-NMR spectrometer was utilized to carry out the proton NMR characterization of the samples in deuterated solvents.

2.4 X-ray Crystallographic Studies

The X-ray data was collected using the SMART X2S single X- ray diffractometer using the Mo-Kα radiation. Single crystals of all compounds were selected under a microscope and mounted on sample pins. The AXS program from Bruker, was used to interpret and integrate the X-ray images of samples. The structures where refined and solved using direct methods on the Burker SHELXTL software package. The final structure was refined anisotropically. The x-ray report was generated from a total of 2160 frames that were collected. The total exposure time was 36.00 hours. The integration of the data using a monoclinic unit cell yielded a total of 14464 reflections to a maximum θ angle of 25.08° (0.84 Å resolution), of which 4680 were independent (average redundancy 3.091, completeness = 98.9%, Rint = 14.54%, Rsig = 14.42%) and 3970 (84.83%) were greater than $2\sigma(F^2)$. The final cell constants of a = 17.4266(14) Å, b = 10.8224(10) Å, c = 18.0270(16) Å, β = 109.309(3)°, volume = 3208.6(5) $Å^3$, are based upon the refinement of the XYZ-centroids of 4577 reflections above 20 σ(I) with 4.499° < 2θ < 49.82°. The ratio of minimum to maximum apparent transmission was 0.358.

The calculated minimum and maximum transmission coefficients (based on crystal size) are 0.0324 and 0.0324. The structure was solved and refined using the Bruker SHELXTL software package. The final anisotropic full-matrix least-squares refinement on F2 with 379 variables converged at R1 = 8.72%, for the observed data and wR2 = 19.15% for all data.

The goodness-of-fit was 0.992. The largest peak in the final difference electron density synthesis was 4.646 $e^-/Å^3$ and the largest hole was -2.657 $e^-/Å^3$ with an RMS deviation of 0.496 $e^-/Å^3$. On the basis of the final model, the calculated density was 4.066 g/cm^3.

2.5 Photoluminescence Measurement

The photoluminescence data was collected using a photon technology international (PTI) spectrometer (model QM-7/SE), the excitation source was a high intensity xenon lamp. The computer "QUADRASCOPIC" monocromators assisted in the selection of the emission and excitation wavelengths. A PMT (Model 928) detector was utilized to carry out signal detection in either the digital or photon counting modes. Both solid and liquid samples were able to be studied at both ambient and low temperatures (liquid nitrogen temperatures). Data were collected both for the emission and excitation spectra using the available protocol provided PTI. Data manipulation was achieved by the FeliX32 fluorescence package. This instrumentation was set up in a dark room to avoid possible interference from visible light and both solid powder and crystalline samples were introduced into the luminescence instrument by means of sealed borosilicate capillary tubes. For samples measurement under liquid nitrogen, cold finger Dewar flask was used.

CHAPTER 3

Results and Discussion

3.1 Crystal Structure of $[Tb(TPAO)_2(H_2O)_4\ (Au(CN)_2)_3]$

The crystal structure of the $[Tb(TPAO)_2(H_2O)_4Au(CN)_2)_3]$complex shown in Figure 3.1 reveals the successful coordination of terbium to two TPAO units, four H_2O molecules, and two C-N groups that links the triangular Au-Au-Au units. (Figure 3.1).Selected bond angles of the crystal structure of the $[Tb(TPAO)_2(H_2O)_4Au(CN)_2)_3]$complex are shown in Table 3.3.

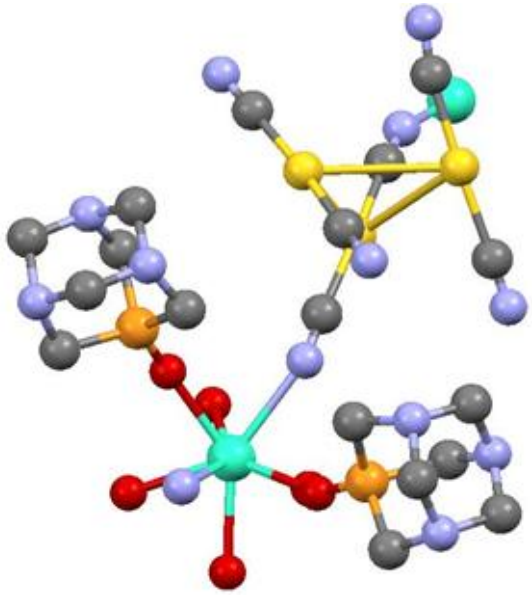

Figure 3.1. X-ray crystal structure of the $[Tb(TPAO)_2(H_2O)_4(Au(CN)_2)_3]$complex.

In the $[Tb(TPAO)_2(H_2O)_4Au(CN)_2)_3]$complex (figure 3.1), the blue atoms represent the nitrogen, the turquoise atoms represent the terbium, the gray atoms represent the carbons, the four free red atoms represent four water molecules directly attached to the terbium core, the orange atoms represent the phosphorus, that connect the two TPAO onto terbium through oxygen atoms represented by two red atoms as well, and the yellow atoms represent the gold, the crystal structure of $[Tb(TPAO)_2(H_2O)_4Au(CN)_2)_3]$ also reveals polymeric strands through the cyanide backbone. (See table 3.1 for X-ray report).

Table 3.1

Summary of X-ray report [$Tb(TPAO)_2(H_2O)_4Au(CN)_2)_3$]

Identification Code	$[Tb(TPAO)_2(H_2O)_4(Au(CN)_2)_3]$
Chemical formula	$TbC_{18}H_{32}Au_3N_{13}O_6P_2$
Formula weight (g/mol)	1338.3
Crystal size (mm)	0.40 x 0.40 x 0.40
Crystal system	monoclinic
Space group	C c
Unit cell dimensions	a = 17.4266(14) Å α = 90° b = 10.8224(10) Å β = 109 c = 18.0270(16) Å γ = 90°
Density (g/cm^3)	4.066
R1	0.0872
wR2	0.1915
Abs. coeff. (mm^{-1})	27.294
Z	4
F	3420
Goodness of fit	0.992
Temperature (K)	200(2)
Wavelength (Å)	0.71073
Volume (Å)	3208.6(5)
Crystal habitat	colorless block

The structure crystallizes in a monoclinic C- c space group, with a Z value of 4. Selected bonds lengths are given in Table 3.2. Notice the CN bridges are slightly shorter (C4-N19= 1.09(4) Å) than the non bridging CN functionalities attached to the gold atoms C2-N6= 1.12(5).

Table 3.2

Selected bond lengths in (Å)

Selected Bond Lengths	(Å)
Au1-Au4	3.145(2)
Au01-Au03	3.2249(15)
Au03-Au04	3.2429(19)
C4-N19 (bridge)	1.09(4)
N8-C23 (bridge)	1.10(4)
C2-N6	1.12(5)
Au1-C4	2.01
Tb1-O8	2.30
Tb1-N8	2.56
Au3-C2	2.02
P2-O8	1.50
P2-C9	1.80
C3-N7	1.12
N19-Tb1	2.57
N15-C17	1.46
P2-C11	1.88(3)
N17-C20	1.52(6)

Table 3.3

Selected bond angles (º)

Selected bond angles	(◦)
C17-N15-C21	109.(3)
C17-N15-C15	113.(2)
C21-N15-C15	113.(2)
N14-C11-P2	108.(2)
N6-C2-Au03	170.(4)
O1-P3-C14	119
C18-P3-C15	100
C4-Au1-C23	171
C4-Au1-Au4	104
O8-Tb1-O1	122
O8-Tb1-N8	70.8
N8-Tb1-N19	110
C2-Au3-C16	177
P3-O1-Tb1	151
O8-P2-C10	118
C10-P2-C9	101

The structure consist of two TPAO molecules coordinated onto the terbium inner core and have a bond angle of 122^0. However there were still four water molecules coordinated onto Tb^{3+} inner sphere position a challenge to our goal of synthesizing water free lanthanide complexes. In addition of the two TPAO ligands, one $Au(CN)_2^-$ acts as a bridge between two

Tb^{3+} centers. Ours and other groups have been studying these types of coordination for possible utilization in biochemistry and in energy sensitization [32] application. The complex $[Tb(TPAO)_2(H_2O)_4Au(CN)_2)_3]$ show the coordination of three gold atoms in a nearly equilateral triangular planar fashion and thus have almost equal bond angles of about 60 degrees (58.2,60.6,61.2). As shown on the Figure 3.2 below.

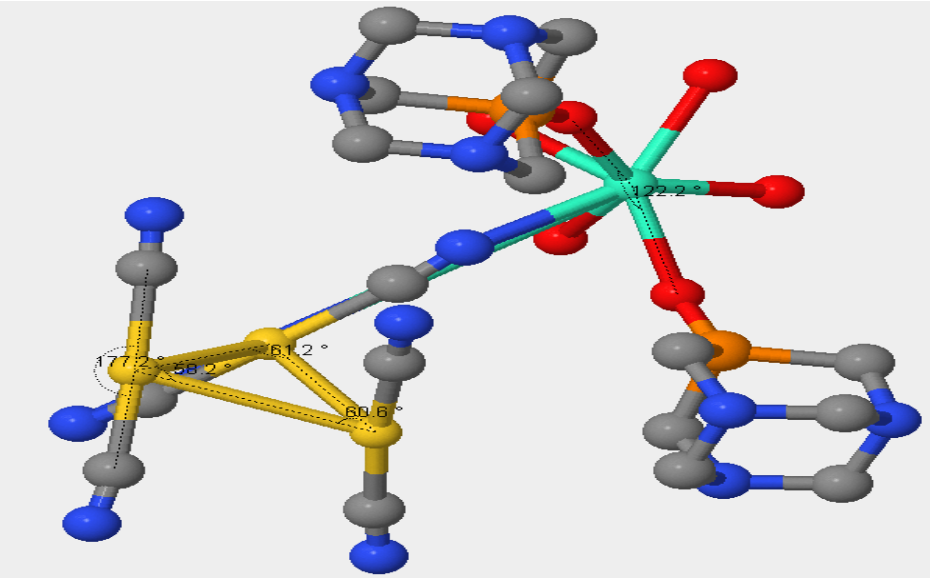

Figure 3.2. Selected bond angles of $[Tb(TPAO)_2(H_2O)_4(Au(CN)_2)_3]$ complex.

The structure of the $[Tb(TPAO)_2(H_2O)_4(Au(CN)_2)_3]$ complex exhibits a unique sequence of polymeric strands not common to these types complexes. It shows repeating units linked together by C-N groups. The structure reveals that one of the three $Au(CN)_2^-$ units is involved in the formation of a one dimensional coordination polymer linking the Tb units through the cyanide bridging. The other two $Au(CN)_2^-$ units are not involved in the linkage of the Tb units and exist as independent counter anions. Interestingly, all three $Au(CN)_2^-$ units aggregate alternatively forming the typical triangular feature, presumably due to the aurophilic interactions. Overall, the structure consists of two potential donor units namely the $Au(CN)_2^-$ and the TPAO, coordinated onto the lanthanide inner coordination sphere. As a result some water molecules

were eliminated, Thus the elimination of (some) H_2O molecules enhances the luminescence intensity and as a consequence, sensitization via energy transfer, becomes efficient.

The $[Tb(TPAO)_2(H_2O)_4(Au(CN)_2)_3]$ reveals a fascinating multi dimensional geometry and can be described as a coordination polymer where the cyanide bridges the transition metal Au and the lanthanide Tb providing an extended one dimensional chain. The complex displays an equilateral gold-gold-gold triangular framework incorporating TPAO ligands onto the terbium inner sphere. As seen in Figure 3.3 below, this complex has some interesting attributes; the three Au-Au bond lengths are 3.14, 3.22 and 3.24 Å.

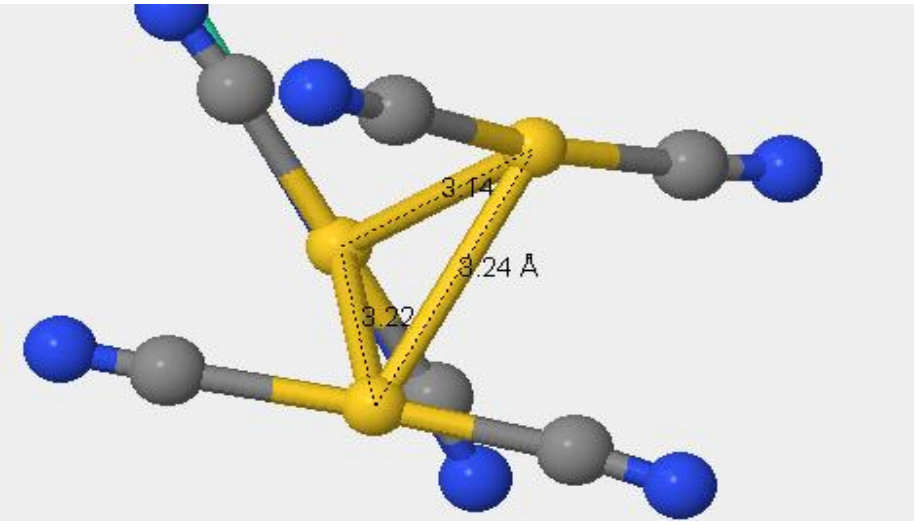

Figure 3.3. Part of the structure of the Tb complex, showing Au-Au-Au bond length in triangular fashion.

These Au-Au bond distances are within the range exhibited for systems showing aurophilic metal-metal interactions. The CN triple bond distance is the shortest length in the lattice with a value of 1.02 Å. With the CN bridging the terbium and gold atoms being the shortest. Formation of equilateral and equiangular geometry for Au-Au-Au is not new in the literature and has previously been established[13, 20, 33, 34], with the Au-Au-Au average bond angles of ~60^0 ,this is seen mainly in gold cluster systems and gold atoms organized around a

main group element [32, 34, 35]. However, this aspect of organization is exhibited for the first time in cyanide bridge coordination polymeric systems [13, 32] of gold complexes.

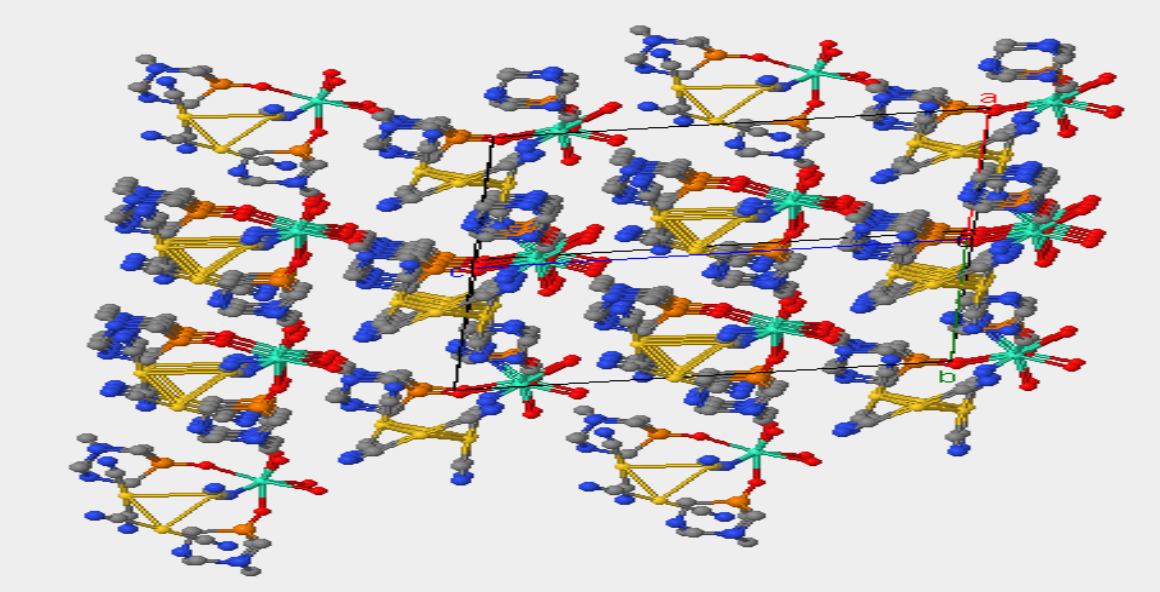

Figure 3.4. Packing diagram of [Tb $(TPAO)_2(H_2O)_4(Au(CN)_2)_3$]

Search in the Cambridge data base with a key word of "triangular gold" reveals a total of 283 hits. These structures include cluster units organized around phosphine ligands and main group elements. There are also few molecular species where the gold atoms are organized through bridging coordination to transition metals. When a refined search was done with "triangular gold" key word containing Au-C bond the result provided only 27 hits. Out of these hits seven structures are compared in Table 3.4 with that of terbium system.

The structures reported by Che chi Ming and others [18] reveal that this complex, has a comparable bond distances when compared with compounds of similar geometric class. Chi-Ming has reported a dinuclear luminescent gold cluster , where a three isosceles triangular gold is embedded in the crystal structure , with intramolecular Au-Au distance of 3.083 and 3.167Å , this distances compares fairly with our findings, although, our Au-Au-Au interaction is unique in its almost equiangular and equidistant morphology.

Balch [34] has also reported the crystal structure of a cyclic trinuclear organo gold complex, Au_3-$(PhCH_2N{=}COMe)_3$, which he reveals, complex does not associate into a trigonal prismatic array via intermolecular interactions of gold(I), this is similar to our work with aurophilic interaction amongst the gold atoms.

Further, Katshukawa [35] has also put forward a series of mixed metal gold phosphine clusters with highly asymmetric skeleton with significant intramolecular aurophilic interactions, with similar bond angles and lengths to our work. The table below shows the bond angles and distances of the crystal $[Tb(TPAO)_2(H_2O)_4(Au(CN)_2)_3]$, compared with other structures from the Cambridge data base. The Au-Au- Au interaction could be described as a molecular triangle consisting of metallic bonds with aurophilic interactions.

Table 3.4

Comparison of bond angles and bond distances of the Au-Au-Au interactions.

Au-Au-Au (triangle)	Bond angle (°)	Bond distance (Å)
Chi-Ming et al. [20]	58.2-60.8-60.8	3.16-3.16-3.08
Siemeling et al. [36]	59.15-61.51-59.33	3.35-3.27-3.28
Mohamad et al. [33]	59.41-61.61-59.43	3.28-3.28-3.33
Vincente, J. et al. [37]	64.72-60.14-55.14	3.30-3.19-3.02
Katsukawa et al. [35]	59.4-58.56-62.01	2.77-2.80-2.90
Balch et al. [34]	58.26-61.61-60.32	3.31-3.36-3.24
Katsukawa et al. [38]	61.40-59.15-59.45	3.25-3.32-3.24
Our work		
Assefa Z. and Forcha D.	58.20-60.62-61.19	3.10-3.22-3.24

In the structure the C-Au-C interaction is nearly linear with a C2-Au3-C16, bond angle of about 177 degrees (almost linear), this findings is in sync with earlier works by Assefa et al [32, 39].

This aspect of coordination of lanthanides to a C-N functionality has been previously mentioned to be of relevance and constitute a family of closely related compounds known as lanthanide cyano aurates $Ln[Au(CN)_2]_3$ and also that the $[Au(CN)_2]^-$ has shown to photosensitize terbium in both the solid and liquid states [32, 39]. Further, the Au-Au-Au connection is shown to have a unique position in the crystal lattice, occupying a somewhat peripheral position in the lattice , while at the same time constitute the framework of the polymeric units as the triangular Au-Au-Au connects via C-N units to bridge two terbium core atoms.

A sectional view of the Au-Au-Au interaction, showing the coordination of two Au atoms to two CN functionality with an almost linear angular arrangement of C-Au-C of 177 degrees and NC-Au of 172 degrees. Figure 3.5.

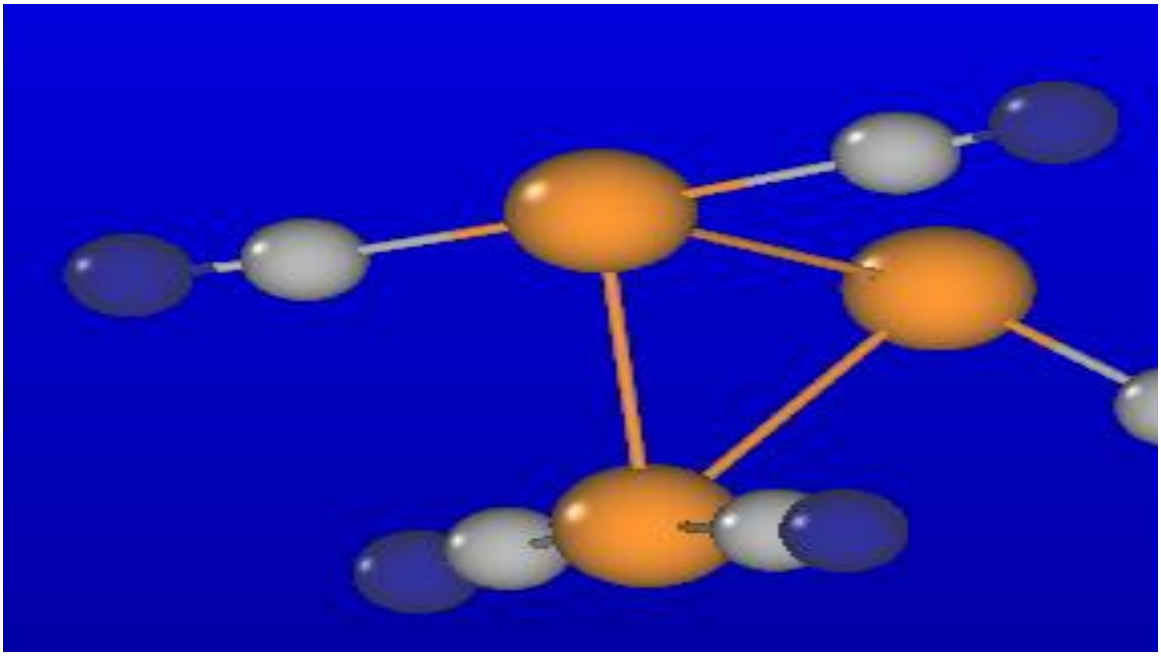

Figure 3.5. Sectional view of the Au-Au-Au interaction, showing coordination.

The thermal ellipsoid diagram in figure 3.6 shows a triangular Au-Au-Au bond in a sequence. The ellipsoids of the nitrogen atoms appear large presumably due to thermal motion in the lattice. Another fascinating attribute of these complexes, is that they are luminescent, and also that the Au-Au aurophilic interaction does play a vital role in the luminescent property of the $[Tb(TPAO)_2(H_2O)_4(Au(CN)_2)_3]$ complex.

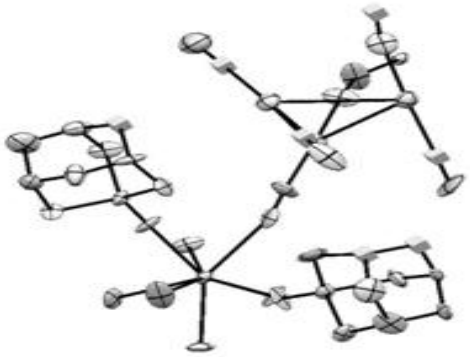

Figure 3.6. Thermal ellipsoid model showing a triangular gold in sequence.

In fact, these complex can be used as building units for the making of polymeric structures with metal-ligand luminescent capabilities as envisaged in the X-ray structure. Infact looking at the interaction between the C-N group and the Au atoms we can make the assertion that the transition that exist in this system is assigned to π-π* transition, within the TPAO ligand and thus transfer some energy to the terbium, and similarly from the metal centre.

3.2 Photoluminescence Studies of $[Tb(TPAO)_2(H_2O)_4(Au(CN)_2)_3]$

The emission spectrum of $[Tb(TPAO)_2(H_2O)_4(Au(CN)_2)_3]$ complex was carried out at room temperature and the excitation wavelength was fixed at 312 nm while the emission range was set between 340-600 nm. A series of peaks were observed. The most intense peak was observed at 541 nm and at 488 nm meanwhile a much weaker band was identified at 588 nm. The emission spectrum of the complex $[Tb(TPAO)_2(H_2O)_4(Au(CN)_2)_3]$, reveals a series of line-like spectrum as can be seen in figure 3.7.

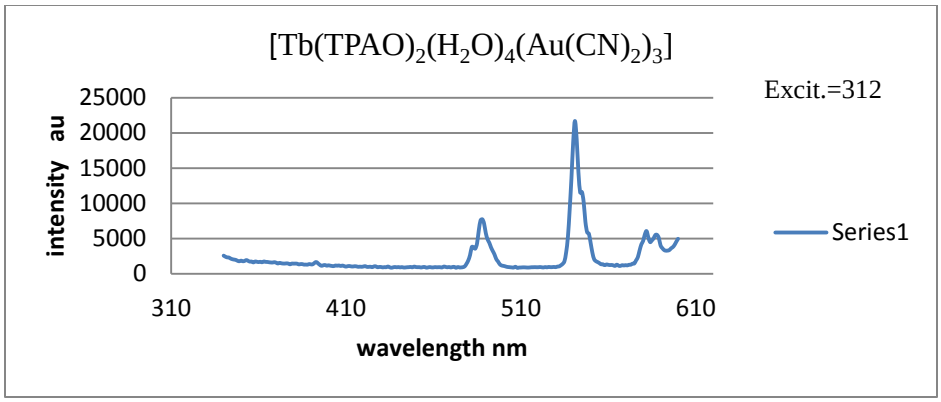

Figure 3.7. Emission spectrum for $[Tb(TPAO)_2(H_2O)_4(Au(CN)_2)_3]$.

The bands were assigned as shown in the table below, for the emission spectrum of $[Tb(TPAO)_2(H_2O)_4(Au(CN)_2)_3]$ The above spectrum shows multiple emissions, with maxima at around 541nm and a dual minimum at around 488 and 582 nm, which corresponds to $^5D_4 \rightarrow ^7F_5$, $^5D_4 \rightarrow ^7F_6$, and $^5D_4 \rightarrow ^7F_4$ transitions, respectively.

Table 3.5

Bands for the emission spectrum of $[Tb(TPAO)_2(H_2O)_4(Au(CN)_2)_3]$.

Energy cm^{-1}	Wavelength	Assigned bands
20747	482	$^5D_4 \rightarrow ^7F_7$
20491	488	$^5D_4 \rightarrow ^7F_6$
25773	388	$^5D_4 \rightarrow ^7F_8$
18484	541	$^5D_4 \rightarrow ^7F_5$
17006	588	$^5D_4 \rightarrow ^7F_3$
17182	582	$^5D_4 \rightarrow ^7F_4$

The excitation spectrum of the complex $[Tb(TPAO)_2(H_2O)_4(Au(CN)_2)_3]$ shows a very broad band maximizing at 313 nm. Observance of a donor excitation band while monitoring the Tb^{3+} emission is indicative of an energy transfer process from the ligand and the metal excited

state. The emission bands which originate from the $^5D_4$ excited level to the various ^7F_J manifolds, are characteristic transitions unique to the Tb^{3+} ion. Sensitization from the Au-Au interaction to the terbium, could be possible since the excitation spectrum, has a broad shoulder extending ~360nm, which overlaps with the absorption region of Au (I) complexes [34, 40].

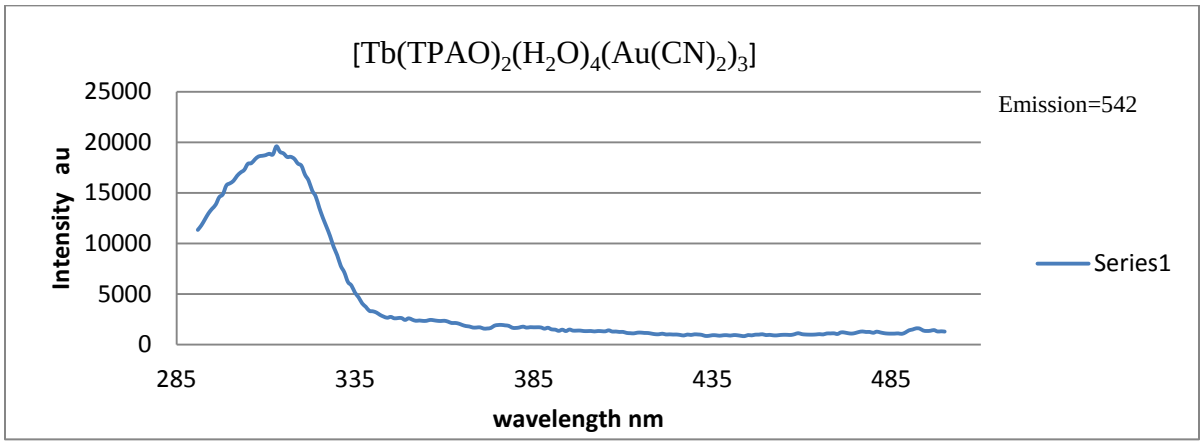

Figure 3.8. Excitation spectrum for **[**$Tb(TPAO)_2(H_2O)_4(Au(CN)_2)_3$**]**.

3.3 Infrared Spectrum of $[Tb(TPAO)_2(H_2O)_4(Au(CN)_2)_3]$

IR data were collected for the sample at ambient condition and thus indicates the presence of different functional groups that are characteristic of the $[Tb(TPAO)_2(H_2O)_4(Au(CN)_2)_3]$ complex. A cyanide stretch is observed at 2150cm^{-1} meanwhile the hump at 2300 cm^{-1} there is a broad band at 3300cm^{-1} indicating νOH, stretching, there is also a P=O around 1050 cm^{-1}.

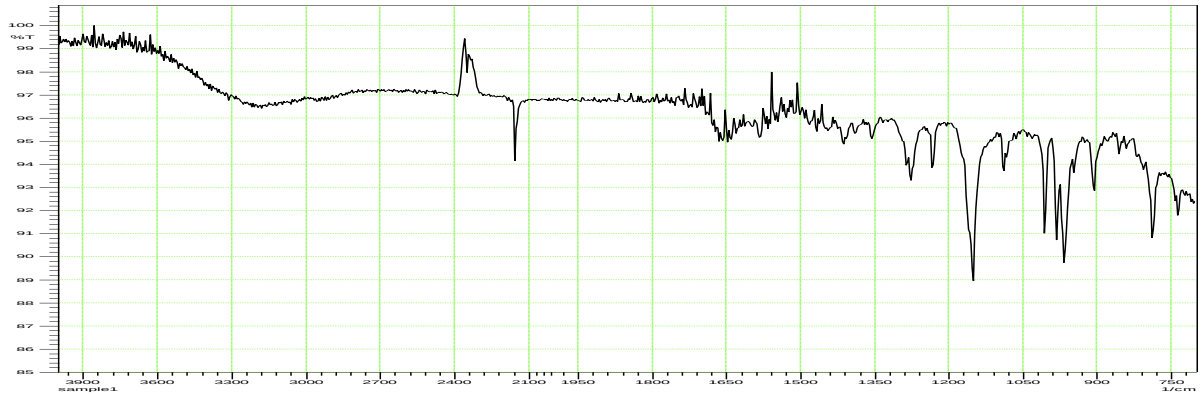

Figure 3.9. Infrared spectrum of $[Tb(TPAO)_2(H_2O)_4(Au(CN)_2)_3]$.

3.4 Photoluminescence Studies of $[Eu(ptpy)(H_2O)_n]Cl_3$ complex

The complex was achieved by coordinating the ligand ptpy, Figure 3.11, with europium cation to obtain the product complex $[Eu(ptpy)(H_2O)_n]Cl_3$ in good yield. After collecting the final product, which was a microcrystalline material, the emission spectrum below was carried out at ambient conditions and the excitation wavelength was held fixed at 383nm and the emission range was set at 403-710 nm, this spectrum indicates a series of sharp peaks unique to the type of transitions that are common for Europium complexes, see Table 3.6 below.

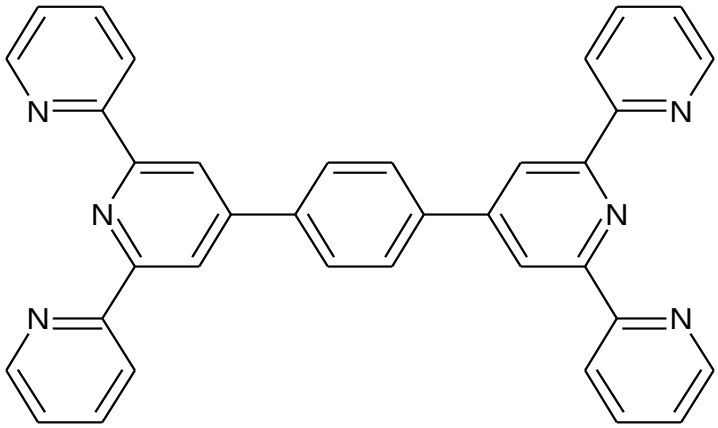

Figure 3.10. Structure of ptpy (4', 4''''- (1-4 phenylene) bis (2, 2':6', 2-terpyridine)).

The most intense emission maxima occur at about 611nm; this could be attributed to transitions originating from the $^5D_0 \rightarrow {}^7F_2$ state, corresponding to the hypersensitive transition, unique to the red emission that is seen for the europium ion. Meanwhile the emission minima occur at 578 and 651nm, which could be ascribed to the $^5D_0 \rightarrow {}^7F_0$ and $^5D_0 \rightarrow {}^7F_3$ transitions respectively, are less intense bands. There is also the possibility of the coordination of some water molecules on to the europium inner coordination sphere and as a result of these molecular vibrations from water molecules, a decrease in the luminescence intensity is likely to be expected for this complex.

Table 3.6

Assignment of the emission spectral band $[Eu(ptpy)(H_2O)_n]Cl_3$.

Energy cm^{-1}	Wavelength(nm)	Assigned transitions
17301	578	$^5D_0 \rightarrow {}^7F_0$
16978	589	$^5D_0 \rightarrow {}^7F_1$
16366	611	$^5D_0 \rightarrow {}^7F_2$
16260	615	$^5D_0 \rightarrow {}^7F_2$
15360	651	$^5D_0 \rightarrow {}^7F_3$
14347	697	$^5D_0 \rightarrow {}^7F_4$

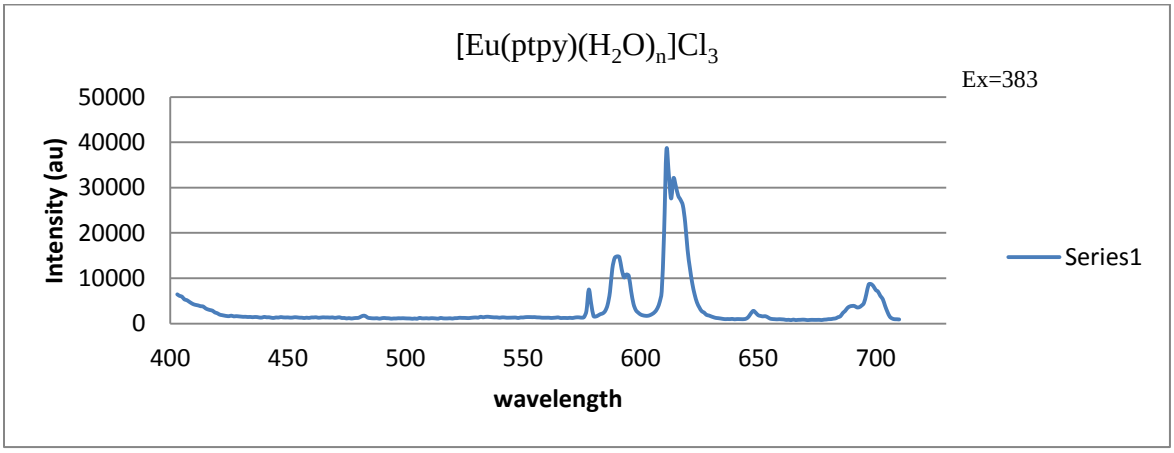

Figure 3.11. Emission spectrum of $[Eu(ptpy)(H_2O)_n]Cl_3$.

The excitation spectra was conducted at room temperature with the emission wavelength held constant at 615 nm and the excitation range was between 330-590 nm, the broad spectral intensity at 382 nm, is indicative of energy transfer from the organic chromophores (ptpy) to the Eu^{3+} as seen on the figure 3.12. This broad peak that is envisage at around 382 nm has a steep shoulder that slants from the maxima to about 420 nm, hence within a 30 nm wide region the intensity of the complex was significantly reduced.

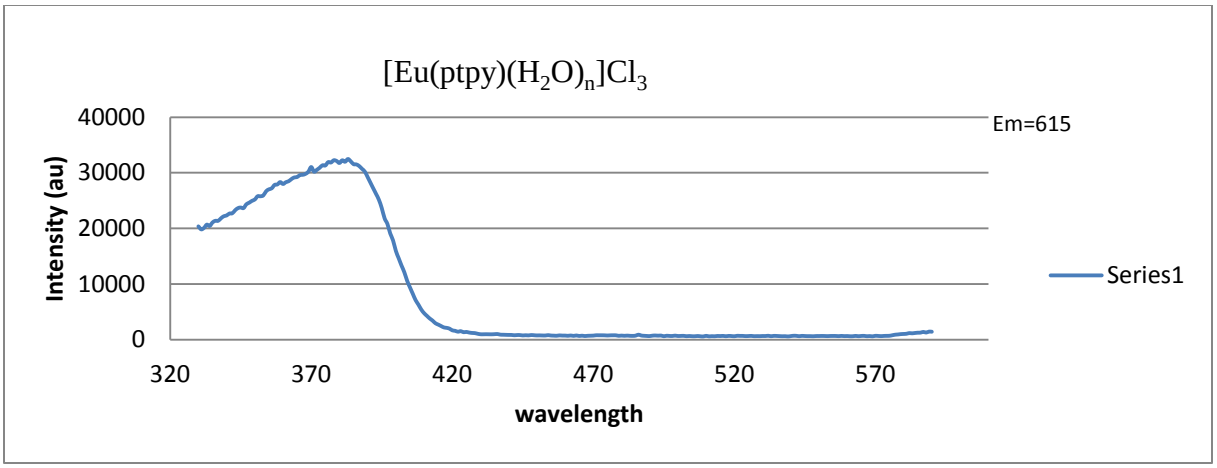

Figure 3.12. Excitation spectrum of $[Eu(ptpy)(H_2O)_n]Cl_3$.

3.5 Infrared spectrum of $[Eu(ptpy)(H_2O)_n]Cl_3$

The IR spectra below reveal some relevant characteristic features that are necessary for the identification of different functional groups, in this complex.Owing to the fact that this complex has the ptpy ligand with conjugated double bonds, various vibrational modes were identified, these are 3300 cm^{-1}, 1650 cm^{-1}, 1600 cm^{-1}, and 1500 cm^{-1}, which corresponds to O-H, C=C, C=C aromatic and aromatic C=C bending vibrations respectively.

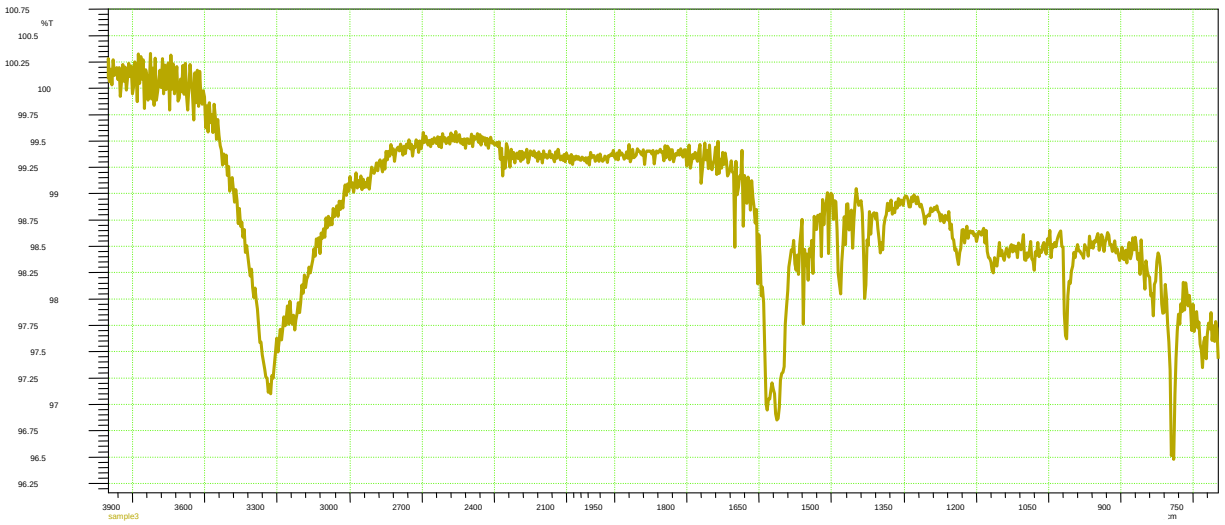

Figure 3.13. Infrared spectrum of $[Eu(ptpy)(H_2O)_n]Cl_3$.

3.6 Photoluminescence Studies of $[Eu(bbterp)(H_2O)_3]Cl_3$

Complexation of the ligand bbterp (figure 3.14) and Eu^{3+} was achieved as solid micro crystalline material that was show to have luminescence. The photoluminescence studies were carried out at room temperature conditions and reveal yet again a series of intense sharp spectral lines that are characteristic of the f-f transition in Eu^{3+} complexes.

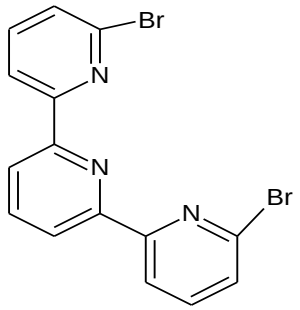

Figure 3.14. Structure of bbterp (6,6″-Dibromo-2,2′:6′,2″-terpyridine)

However some weak bands do appear, at 651cm^{-1} and at 689 cm^{-1}, while the strong sharp spectra lines are at 578 cm^{-1}, 590 cm^{-1}, 610 cm^{-1}, 615 cm^{-1} and 697 cm^{-1}. These bands have been assigned as seen on Table 3.7 below.

Table 3.7

Assignment of emission bands for $[Eu(bbterp)(H_2O)_n]Cl_3$complex

Energy cm^{-1}	Wavelength(nm)	Assigned bands
17301	578	$^5D_0 \rightarrow {}^7F_0$
16949	590	$^5D_0 \rightarrow {}^7F_1$
16393	610	$^5D_0 \rightarrow {}^7F_2$
16260	615	$^5D_0 \rightarrow {}^7F_2$
15360	651	$^5D_0 \rightarrow {}^7F_3$
14347	697	$^5D_0 \rightarrow {}^7F_4$

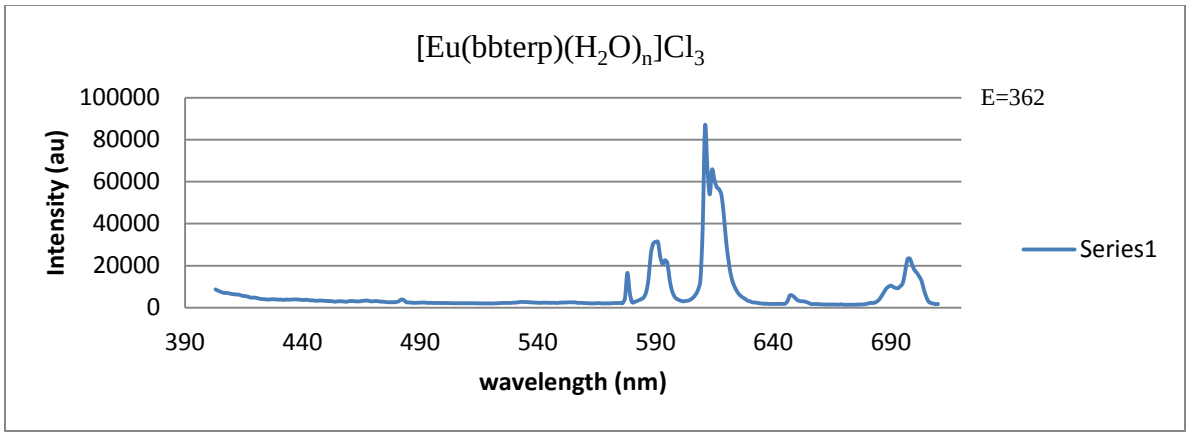

Figure 3.15. The emission spectrum of $[Eu(bbterp)(H_2O)_n]Cl_3$.

The emission spectrum above shows several bands. Some of these bands are sharp line like bands such as observed at 578 nm, 590 nm, 610 nm and 697 nm. The excitation spectrum was done at 25 ^{0}C and while the emission wavelength was held constant at 615 nm and the excitation range was between 330-590 nm, the broad spectral intensity at around 370 nm, Figure 3.17, in this region is indicative of ligand to metal energy transfer process, resulting from the interaction of the brominated organic chromophores (bbterp) with the Eu^{3+} ion. Further, the broad spectrum around 370,401,472 and 485 nm could also be ascribed to the f-f transitions as seen in Table 3.8 below.

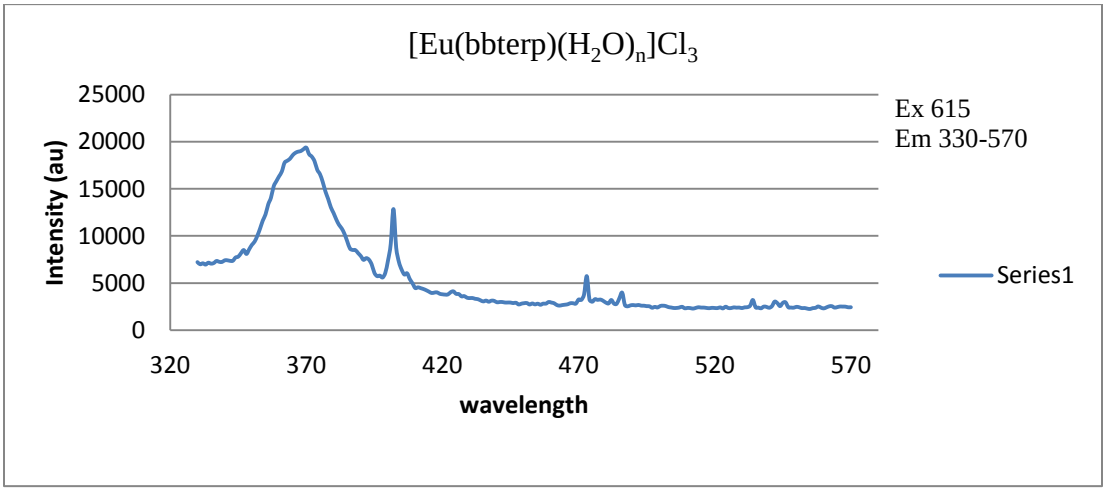

Figure 3.16. The excitation spectrum of $[Eu(bbterp)(H_2O)_n]Cl_3$.

Table 3.8

Assignment of excitation bands of the [Eu(bbterp)(H_2O)$_n$]Cl_3complex.

Energy cm^{-1}	Wavelength(nm)	Assigned bands
27027	370	$^7F_0 \rightarrow {}^5L_6$
24938	401	$^7F_0 \rightarrow {}^5D_2$
21186	472	$^7F_0 \rightarrow {}^5D_2$
20618	485	$^7F_0 \rightarrow {}^5D_1$

3.7 Infrared spectroscopy of [Eu(bbterp)(H_2O)$_n$]Cl_3.

The IR data below strongly suggest the presence of OH vibrational stretching a well as saturated aromatic C=C , NH vibrational modes, these corresponds to the broad band at about 3300 cm^{-1}, 1600 cm^{-1} and 3500 cm^{-1} respectively.

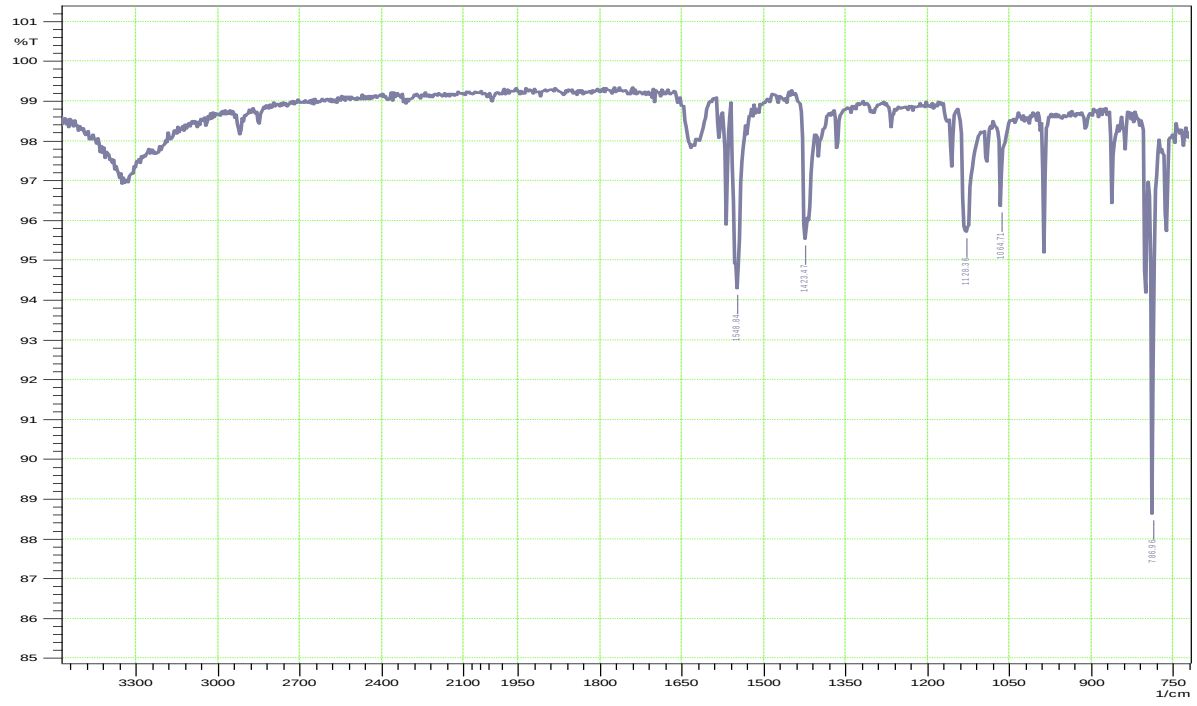

Figure 3.17. Infrared spectrum of [Eu(bbterp)(H_2O)$_n$]Cl_3.

3.8 Photoluminescence Studies of $[Eu(ppz)_2(H_2O)_n]Cl_3$

The complex $[Eu(ppz)_2(H_2O)_n]Cl_3$ was obtained in good yield as small crystals, not quite suitable for crystal work however, effort by our research group, have been able to confirm the structure of this complex by other means like IR and Luminescence spectroscopy. The photoluminescence spectra observed for the $[Eu(ppz)_2(H_2O)_n]Cl_3$ complex is shown below.

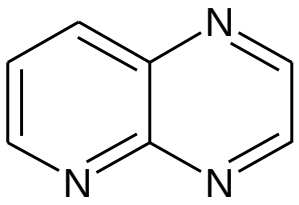

Figure 3.18. Structure of the ppz (Pyridino [2-3-b] pyrazines)

The excitation spectrum was done with the emission wavelength held fixed at 615 nm. The spectrum was collected and the emission wavelength range was from 330 to 590nm, under room conditions of temperature and pressure. The emission spectrum indicates a broad peak at around 364nm, further such a broad spectrum is indication of energy transfer and subsequent luminescence of the complex.

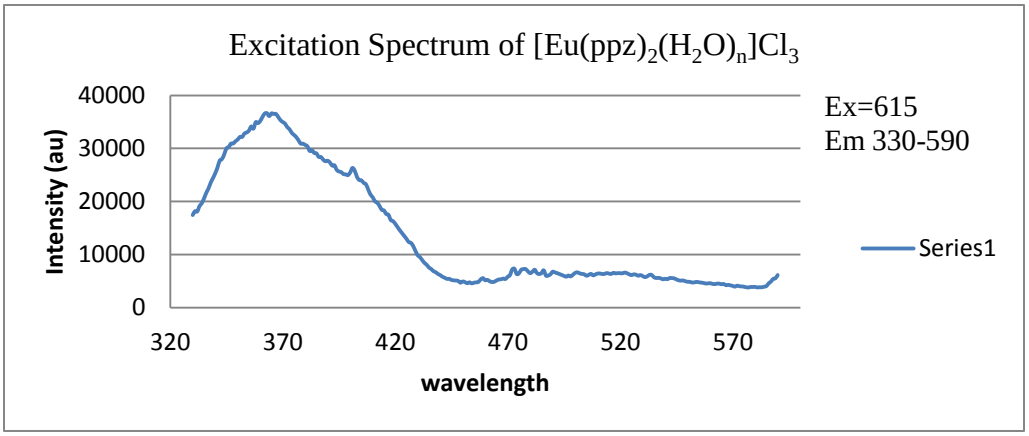

Figure 3.19. Excitation spectrum of $[Eu(ppz)_2(H_2O)_n]Cl_3$.

The emission spectrum of $[Eu(ppz)_2(H_2O)_n]Cl_3$ carried out under ambient conditions, reveal a couple of sharp spectral lines indicative of the f-f transition common to Eu^{3+} complexes. There are also weak bands that can be identified at 454nm and 577nm, corresponding to the $^5D_0 \rightarrow {}^7F_0$ transition.

Table 3.9

Assignment of emission bands for $[Eu(ppz)_2(H_2O)_n]Cl_3$.

Energy cm-1	Wavelength	Assigned bands
16367	611	$^5D_0 \rightarrow {}^7F_2$
16260	615	$^5D_0 \rightarrow {}^7F_2$
16949	590	$^5D_0 \rightarrow {}^7F_1$
22026	454	$^5D_0 \rightarrow {}^7F_0$
17331	577	$^5D_0 \rightarrow {}^7F_0$

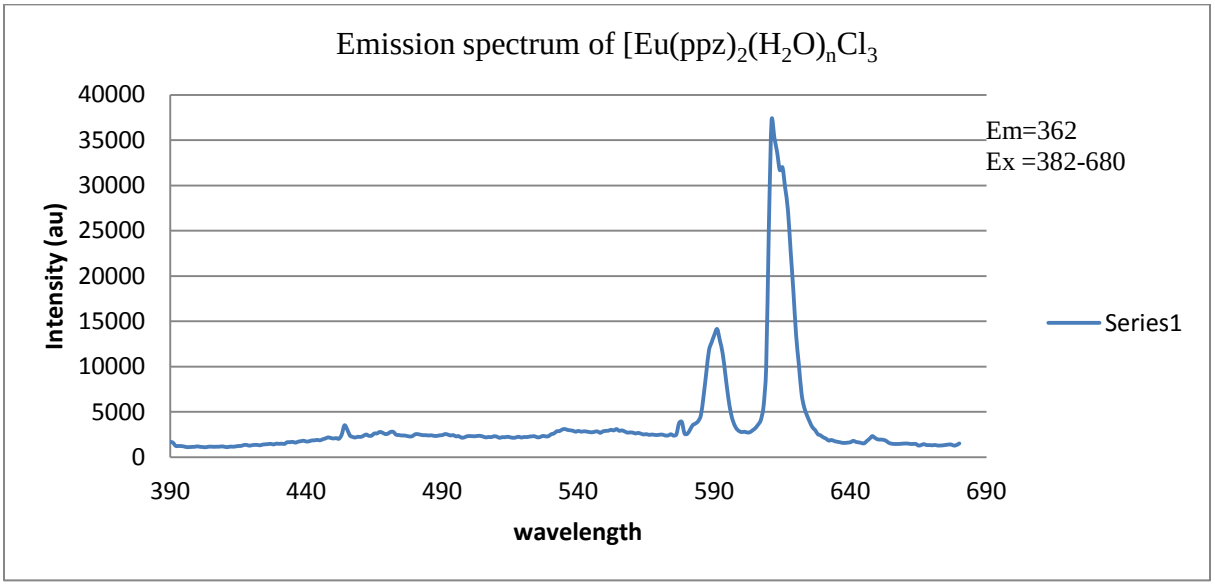

Figure 3.20. Emission spectrum of $[Eu(ppz)_2(H_2O)_n]Cl_3$.

3.9 Infrared spectra of $[Eu(ppz)_2(H_2O)_n]Cl_3$

The IR data was collected from about 600 to 4000 $cm^{-1}$and the frequencies that identify various functional groups where observed, such as at 3300 cm^{-1} for O-H vibrations as well as C-N stretching at 1150 cm^{-1} and also C-H at around 3000 cm^{-1}, as seen on figure below.

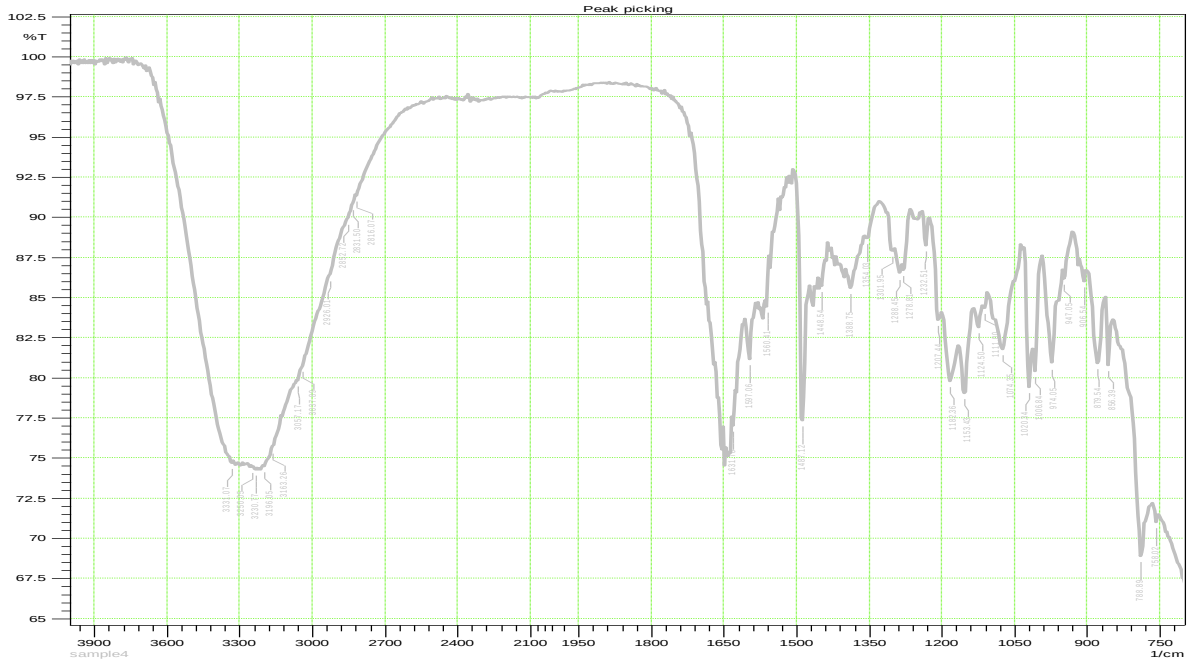

Figure 3.21. Infrared spectrum of $[Eu(ppz)_2(H_2O)_n]Cl_3$.

The results of this work numerates the complexation of four complexes and their excitation bands, that has been put together for a broad comparison, their excitation maxima is well within the UV/VIS region of the electromagnetic spectrum, indicating that the broad band is a consequence of the coordination of the organic chromophores in the complex, this further indicates various excitation spectra as in figure 3.22 below, illustrate the fact that all the complexes, reveal some sort of interaction between the ligand and the europium or terbium cations. As indicated by the broad emission observed around 290 nm through 420 nm, for these complexes, the intensity decrease as you move to higher wavelengths, above the 420 nm, see Figure 3.22 below.

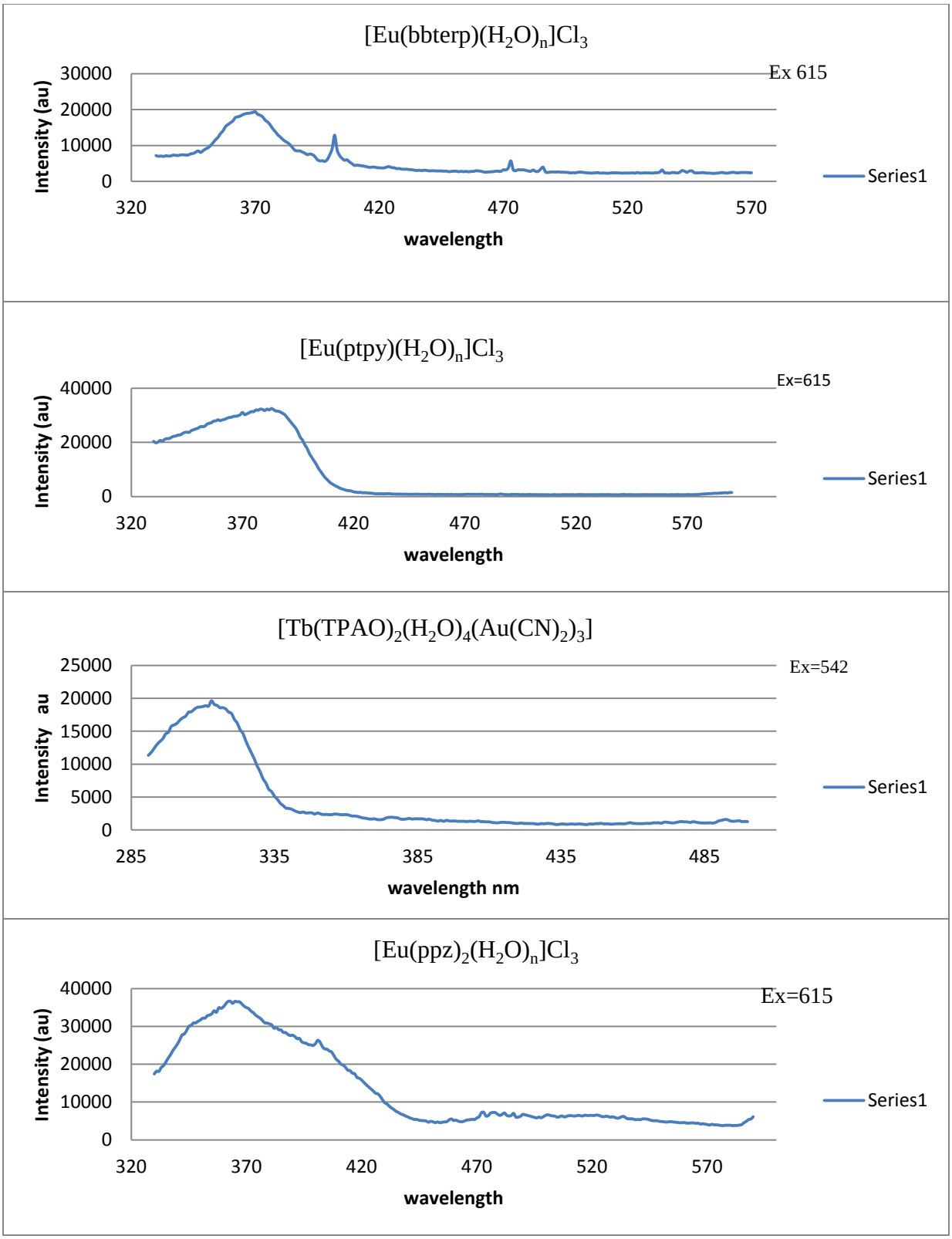

Figure 3.22. Comparison of four complexes and their excitation spectra

3.10 X-ray crystal structure of tetra 2 pyridynyl pyrazine

A colorless block-like specimen of $C_{24}H_{19}N_6$, approximate dimensions 0.40 mm x 0.40 mm x 0.40 mm, was used for the X-ray crystallographic analysis. The X-ray intensity data were measured. A total of 720 frames were collected. The total exposure time was 1.00 hours. The integration of the data using a monoclinic unit cell yielded a total of 5675 reflections to a maximum θ angle of 25.06° (0.84 Å resolution), of which 1667 were independent (average redundancy 3.404, completeness = 98.8%, R_{int} = 4.79%, R_{sig} = 4.59%) and 1200 (71.99 %) were greater than 2σ(F2). The final cell constants of a = 9.849(2) Å, b = 10.147(2) Å, c = 9.918(2) Å, β = 105.875(7)°, volume = 953.4(4) Å3, are based upon the refinement of the XYZ-centroids of 1308 reflections above 20 σ(I) with 5.158° < 2θ < 47.44°. Data were corrected for absorption effects using the multi-scan method (SADABS). The ratio of minimum to maximum apparent transmission was 0.743. The calculated minimum and maximum transmission coefficients (based on crystal size) is 0.9666.

The structure was solved and refined using the Bruker SHELXTL Software Package, using the space group P 2_1/n 1, with Z = 2 for the formula unit, $C_{24}H_{16}N_6$.The instrumentation was also able to reveal the molecular weight of the complex as well as the volume in angstroms, further, the software was able to reveal the densities of the various elements as well as the density of the complex. The final anisotropic full-matrix least-squares refinement on F2 with 136 variables converged at R1 = 3.88%, for the observed data and wR2 = 10.42% for all data.

The goodness-of-fit was 1.041. The largest peak in the final difference electron density synthesis was 0.160 e-/$Å^3$ and the largest hole was -0.172 e-/$Å^3$ with an RMS deviation of 0.040 e-/$Å^3$. On the basis of the final model, the calculated density was 1.374 g/cm^3. A summary of the X-ray data for the tppz crystal is given in table 3.10 below.

Table 3.10

X-Ray data for tppz.

Chemical formula	$C_{24}H_{16}N_6$	
Formula weight	394.48	
Temperature (K)	200(2)	
Wavelength(Å)	0.71073	
Crystal size (mm)	0.40 x 0.40 x 0.40	
Crystal habit	colorless block	
Crystal system	monoclinic	
Space group	P21/n	
Unit cell dimensions	a = 9.849(2) Å	α = 90°
	b = 10.147(2) Å	β = 105.875(7)°
	c = 9.918(2) Å	γ = 90°
Volume	953.4(4) $Å^3$	
R1	3.88	
Resolution (Å)	0.84	
Z	2	
Density (calculated) (g/cm^3)	1.374	
Absorption coefficient(mm^{-1})	0.085	
F(000)	416	
$\Sigma\, w(F_o^2 - F_c^2)^2$, $w=1/[\sigma^2(F_o^2)+(0.0499P)^2+0.0434P]$ where $P=(F_o^2+2F_c^2)/3$		

Table 3.11

Bond lengths for tppz

Bonds	Bond Length(Å)	Bonds	Bond Length(Å)
N1-C5	1.341(2)	N1-C6	1.34
N2-C4	1.33	N2-C7	1.33
N3-C9	1.34	N3-C10	1.34
C1-C2	1.36	C1-C7	1.37
C1-H1	0.95	C2-C3	1.37
C2-H2	0.95	C3-C4	1.38
C3-H3	0.95	C4-C5	1.48
C5-N1	1.34	C5-C6	1.40
C6-C10	1.48	C7-H7	0.95
C8-C9	1.36	C8-C12	1.37
C8-H8	0.95	C9-H9	0.95
C10-C11	1.38	C11-C12	1.38
C11-H11	0.95	C12-H12	0.95

The X-ray data of the crystal structure tetra 2 pyridynyl pyrazines, indicates that the C-H single bonds are the shortest in length as expected ~0.95 Å, meanwhile, the C-C double and the C-N double bonds are ~1.36 and 1.34 Å respectively, there is also the NC bonds of about 1.33 Å in agreement with already established literature values. Further, due to the free rotation of the C-C bond that connects the pyrazine and the pyridine ring, it makes the tetra 2 pyridynyl pyrazines ligand more versatile and can attain multiple conformations.

Table 3.12

Selected bond angles (°) for Tppz.

Bonds	Angles(°)	Bonds	Angles(°)
C9-N3-C10	116	C2-C1-C7	119
C2-C1-H1	120	C7-C1-H1	120
C1-C2-C3	118	C1-C2-H2	120
C3-C2-H2	120	C2-C3-C4	118
C2-C3-H3	120	C4-C3-H3	120
N2-C4-C3	123	N2-C4-C5	115
C3-C4-C5	121	N1-C5-C6	120
N1-C5-C4	115	C6-C5-C4	123
N1-C6-C5	121	N1-C6-C10	114
C5-C6-C10	123	N2-C7-C1	123
N2-C7-H7	118	C1-C7-H7	118
C9-C8-C12	118	C9-C8-H8	120
C12-C8-H8	120	N3-C9-C8	124
N3-C9-H9	118	C8-C9-H9	118
N3-C10-C11	123	N3-C10-C6	115
C11-C10-C6	121	C10-C11-C12	118
C10-C11-H11	120	C12-C11-H11	120
C8-C12-C11	118	C8-C12-H12	120
C11-C12-H12	120		

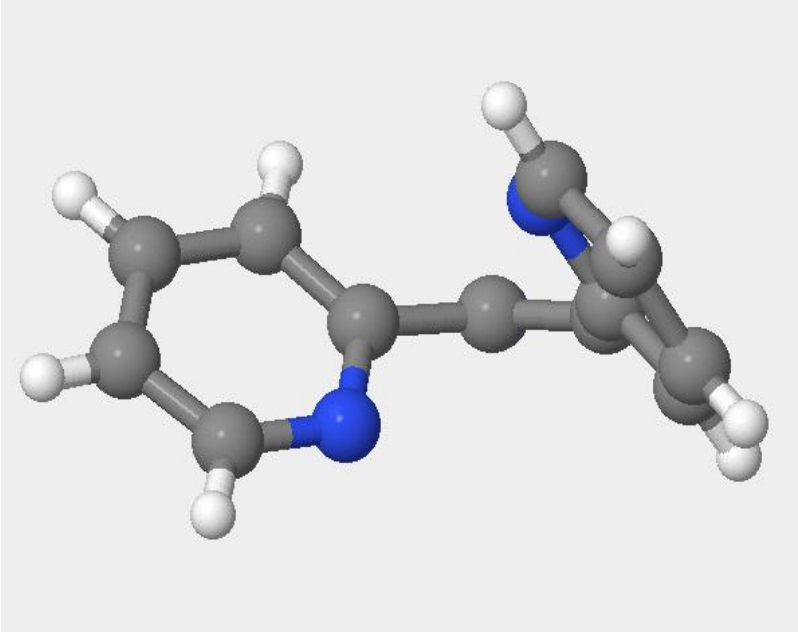

Figure 3.23. Structure of tppz ligand showing the morphology at the edge of the crystal lattice.

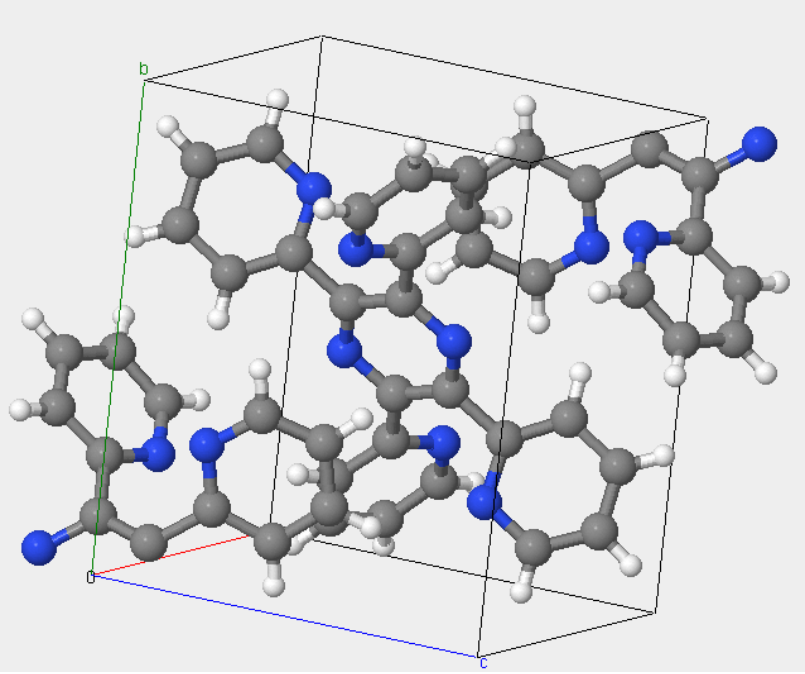

Figure 3.24. X-ray crystal structure of ligand showing distortions of N-donor atoms.

CHAPTER 4

Conclusion

This work shows four new compounds that have been successfully synthesized and characterized, using single X-ray diffraction, photoluminescence and IR spectroscopy, of these structures, two of them gave good quality crystals and the remaining two gave microcrystalline powdered products. Generally, the purpose of this research has been achieved which was to emphasize the sensitization in lanthanide complexes and to illustrate dual donor sensitization.

Amongst the compounds that were synthesized, is $[Tb(TPAO)_2(H_2O)_4(Au(CN)_2)_3]$, complexation of this polymeric compound, is shown a dual donor intramolecular energy transfer. For the two donor groups namely the Au and the TPAO functionalities, our findings here shows that the equilateral triangular gold moiety is connected to the lanthanide cation by bridging C-N groups, and thus is in excellent agreement with established findings, which indicates that group 11 transition metals acting as donor systems, have been shown to undergo energy transfer to some lanthanide cations, with occasional CN acting as bridges between the lanthanides and the transition metals[12]. Of the other structures that where synthesized, namely $[Eu(ppz)_2(H_2O)_n]Cl_3$, $[Eu(bbterp)(H_2O)_n]Cl_3$ and $[Eu(ptpy)(H_2O)_n]Cl_3$, these structures have derivative of the pyrazines and the terpyridines, which interestingly have donor groups that absorb in the UV region and thus have the ability to exhibit energy transfer capabilities, this again is in sync with our research objectives of utilizing ligands with multiple donor groups to act as light harvesting antennae. With reference to the above three structures just mentioned, some interesting conclusions were drawn, it was revealed in the excitation spectra, that a broad spectrum was observed at 369nm,366nm and 380nm respectively for $[Eu(ppz)_2(H_2O)_n]Cl_3$,

$[Eu(bbterp)(H_2O)_n]Cl_3$ and $[Eu(ptpy)(H_2O)_n]Cl_3$ complexes this is a solid indication that there exist a donor – acceptor type of interaction in these systems. In conclusion, this write-up will be an important addition to the mechanism and form an elaborate example of complexes that undergo energy transfer sensitization via organic chromophores to europium and terbium.

References

1. Earnshaw, N.N.G.a.A., *Chemistry of the Elements*. second edition ed1997, UK: Butterworth-Heinmemann. 1340.
2. F. Albert Cotton, G.W., Carlos A. Murillo, Manfred Bochmann, *Advanced Inorganic Chemistry*. Sixth Edition ed1999, New York,NY, USA John Whiley and Sons, Inc.,.
3. Wiberg, H.-. *Inorganic Chemistry*2001, San Diego, CA, USA: Harcourt Science and Technology Co.
4. Cotton, S., *Lanthanides and Actinides*1991, New York: Oxford University Press.
5. Imamoto, T., *Lanthanides in Organic Synthesis*1994. 2.
6. D. F. Shriver, P.W.A., T. L. Overton, J. P. Rourke, M. T. Weller, and F. A. Armstrong, *Inorganic Chemistry*. Fourth Edition ed2006, Great Britain: Oxford University Press.
7. Binnemans, K., *Ionic Liquid Crystals.* Chemical Reviews, 2005. **105**(11): p. 4148-4204.
8. Bünzli, J.-C.G., et al., *New Opportunities for Lanthanide Luminescence.* Journal of Rare Earths, 2007. **25**(3): p. 257-274.
9. Werts, M.H.V., *Making sense of lanthanide luminescence.* Science Progress, 2005. **88**(2): p. 101+.
10. Lakowicz, J.R., *Principles of Fluorescence Spectroscopy*. Third Edition ed2006, NY, United States: Springer Science + Business Media, LLC
11. Bünzli, J.-C.G., et al., *Lanthanide luminescence efficiency in eight- and nine-coordinate complexes: Role of the radiative lifetime.* Coordination Chemistry Reviews, 2010. **254**(21–22): p. 2623-2633.
12. Maynard, B.A., et al., *Intramolecular Energy Transfer in a One-Dimensional Europium Tetracyanoplatinate.* Inorganic Chemistry, 2008. **47**(6): p. 1895-1897.

13. Stojanovic, M., et al., *Structural analysis and photoluminescence properties of low dimensional lanthanide tetracyanometallates.* Inorganica Chimica Acta, 2011. **376**(1): p. 414-421.

14. Vicentini, G., et al., *Luminescence and structure of europium compounds.* Coordination Chemistry Reviews, 2000. **196**(1): p. 353-382.

15. Døssing, A., *Luminescence from Lanthanide(3+) Ions in Solution.* European Journal of Inorganic Chemistry, 2005. **2005**(8): p. 1425-1434.

16. Stwertka, A., *A Guide to the Elements*. Second Edition ed2002, New York, United States: Oxford University Press, Inc.

17. Werts, M.H.V., R.T.F. Jukes, and J.W. Verhoeven, *The emission spectrum and the radiative lifetime of Eu3+ in luminescent lanthanide complexes.* Physical Chemistry Chemical Physics, 2002. **4**(9): p. 1542-1548.

18. Maekawa, M., et al., *Syntheses and structural characterizations of novel mono- and dinuclear iridium hydrido complexes with polydentate nitrogen donor ligands.* Inorganica Chimica Acta, 2004. **357**(12): p. 3456-3472.

19. Smentek, L. and A. Ke¸dziorski, *Efficiency of the energy transfer in lanthanide-organic chelates; spectral overlap integral.* Journal of Luminescence, 2010. **130**(7): p. 1154-1159.

20. Che, C.-M., et al., *Luminescent metal clusters. Spectroscopic properties and X-ray structure of a trinuclear gold(I) complex containing bis(diphenylphosphino)methane and phenylacetylide.* Polyhedron, 1994. **13**(6–7): p. 887-890.

21. http://wolfweb.unr.edu/~abd/f_spectroscopy.shtml.

22. Wells, A.F., *Structural Inorganic Chemistry*. Third Edition ed1962, London, UK: Oxford University Press.

23. Padgett, C.W., W.T. Pennington, and T.W. Hanks, *Conformations and Binding Modes of 2,3,5,6-Tetra(2'-pyridyl)pyrazine.* Crystal Growth & Design, 2004. **5**(2): p. 737-744.

24. Goodwin, H.A. and F. Lions, *Tridentate Chelate Compounds. II1.* Journal of the American Chemical Society, 1959. **81**(24): p. 6415-6422.

25. Grove, H., et al., *Chains and channels in polynuclear copper(II) complexes with 2,3-bis(2-pyridyl)pyrazine (dpp) as bridging ligand; syntheses, crystal structures and magnetic properties.* Inorganica Chimica Acta, 2000. **310**(2): p. 217-226.

26. Swor, C.D. and D.R. Tyler, *Synthesis and coordination chemistry of macrocyclic phosphine ligands.* Coordination Chemistry Reviews, 2011. **255**(23–24): p. 2860-2881.

27. Ashutosh Sharma, S.G.S., *Introduction to Fuorescence Spectroscopy*1999, NY,United States: John Wiley and Sons, Inc.

28. Malta, O.L., *Mechanisms of non-radiative energy transfer involving lanthanide ions revisited.* Journal of Non-Crystalline Solids, 2008. **354**(42–44): p. 4770-4776.

29. Wang, X., et al., *Effect on the fluorescence branching ratio of different synergistic ligands in neodymium complex doped PMMA.* Journal of Non-Crystalline Solids, 2012. **358**(12–13): p. 1506-1510.

30. Carlos, L.D., et al., *Lanthanide-Containing Light-Emitting Organic–Inorganic Hybrids: A Bet on the Future.* Advanced Materials, 2009. **21**(5): p. 509-534.

31. Whitehead, K.E., *Synthesis, Characterisation, and Spectroscopic Studies of Lanthanide Complexes with Potential for Increased Sensitization and Luminescent Enhancement,* in *Chemistry*2011, North Carolina A&T State University: Greensboro, North Carolina.

32. Ladner, L., et al., *Solid-State Photoluminescence Sensitization of Tb3+ by Novel Au2Pt2 and Au2Pt4 Cyanide Clusters.* Inorganic Chemistry, 2011. **50**(6): p. 2199-2206.

33. Mohamed, A.A., et al., *External heavy-atom effect of gold in a supramolecular acid-base [small pi] stack.* Dalton Transactions, 2005. **0**(15): p. 2597-2602.

34. Balch, A.L., M.M. Olmstead, and J.C. Vickery, *Gold(I) Compounds without Significant Aurophilic Intermolecular Interactions: Synthesis, Structure, and Electronic Properties of Ph3PAuC(O)NHMe and Au3(PhCH2NCOMe)3: Comparative Monomeric and Trimeric Analogues of the Solvoluminescent Trimer, Au3(MeNCOMe)3.* Inorganic Chemistry, 1999. **38**(15): p. 3494-3499.

35. Katsukawa, Y., et al., *Syntheses and X-ray structures of mixed-metal gold phosphine clusters including an example having a highly asymmetric Re2Au2 skeleton.* Inorganica Chimica Acta, 1999. **294**(2): p. 255-265.

36. Siemeling, U., D. Rother, and C. Bruhn, *"Schizoid" reactivity of 1,1[prime or minute]-diisocyanoferrocene.* Chemical Communications, 2007. **0**(41): p. 4227-4229.

37. Vicente, J., et al., *Synthesis of Luminescent Alkynyl Gold Metalaligands Containing 2,2'-Bipyridine-5-yl and 2,2':6',2''-Terpyridine-4-yl Donor Groups.* Organometallics, 2008. **27**(4): p. 646-659.

38. Wilton-Ely, J.D.E.T., et al., *The Effect of Hard and Soft Donors on Structural Motifs in (Isocyanide)gold(I) Complexes.* Helvetica Chimica Acta, 2001. **84**(10): p. 3216-3232.

39. Thomas, R.B., et al., *Synthesis, Structural, and Photoluminescence Studies of Gd(terpy)(H2O)(NO3)2M(CN)2 (M = Au, Ag) Complexes: Multiple Emissions from Intra- and Intermolecular Excimers and Exciplexes.* Inorganic Chemistry, 2012. **51**(6): p. 3399-3408.

40. Li, X.-L., et al., *Dual Luminescent Tetranuclear Organogold(I) Macrocycles of 5,5'-Diethynyl-2,2'-bipyridine and Their Efficient Sensitization of Yb(III) Luminescence.* Inorganic Chemistry, 2011. **51**(1): p. 109-118.